THE CRYO-EM STRUCTURE OF THE ΔRIMM IMMATURE 30S SUBUNIT

THE CRYO-EM STRUCTURE OF THE ΔRIMM IMMATURE 30S RIBOSOMAL SUBUNIT: A SNAPSHOT OF THE PROTEIN FACTORY UNDER CONSTRUCTION

By MEREDITH CORRIGAN KENT, B.Sc.

A Thesis Submitted to the School of Graduate Studies
in Partial Fulfillment of the Requirements for
the Degree Master of Science

McMaster University

McMaster University MASTER OF SCIENCE (2012)
Hamilton, Ontario (Biochemistry and Biomedical Sciences)

TITLE: THE CRYO-EM STRUCTURE OF THE ΔRIMM IMMATURE 30S RIBOSOMAL SUBUNIT: A SNAPSHOT OF THE PROTEIN FACTORY UNDER CONSTRUCTION
AUTHOR: Meredith C. Kent, B.Sc. (University of Guelph)
SUPERVISOR: Professor J. Ortega
NUMBER OF PAGES: ix, 64

ABSTRACT

The ribosome is part of the indispensable machinery of every living cell. This large macromolecule, which decodes messenger RNA to produce proteins, is the subject of intense study as the mediator of an essential process. The prokaryotic ribosome is a major target for antimicrobial therapy, as its structure differs significantly from the eukaryotic ribosome. At present, the *in vivo* process of translation on the mature bacterial, or 70S, ribosome is well studied and increasingly understood, while the process of assembling the small (30S) and large (50S) subunits of this complex ribonucleoprotein enzyme has mostly been studied *in vitro*. Consequently, the significance of *in vivo* events such as ribosomal RNA (rRNA) maturation and factor-mediated maturation is incompletely understood. By studying the nature and structure of an *in vivo* assembled immature 30S subunit, this thesis aims to gain a better understanding of the key events in 30S subunit biogenesis. Deletion of the assembly cofactor Ribosome Maturation Factor M (RimM) results in slow growth, inefficient rRNA processing, and accumulation of nonfunctional, immature 30S subunits. This work presents the first cryo-EM model of the immature 30S purified from a RimM knockout strain of *E. coli*. The structure reveals distortion of the decoding centre and a disrupted 50S-binding interface, attesting to the importance of rRNA processing in 30S maturation. Additionally, the model suggests consequences for ribosomal protein incorporation and rRNA domain position relative to the mature 30S.

ACKNOWLEDGEMENTS

I would like to thank my supervisor Dr. Joaquin Ortega for his support and guidance in my pursuit of my graduate degree, and my committee members, Dr. Eric Brown and Dr. Lori Burrows for their valuable advice in this project. Special thanks go to my colleagues in the Ortega Lab, especially to Ahmad Jomaa for his integral contribution to this project in acquiring the cryo-EM images of the Δ*rimM* 30S and for our many discussions, and also to Vivian Leong, for her tireless technical support and advice. I am grateful also to my friend Chris Robertson for proofreading this thesis.

And finally, I'd like to thank my family for their unconditional support in good times and bad, and for setting the gold standard for teamwork under pressure.

Table of Contents

List of Figures and Tables

List of Abbreviations and Symbols

3D	Three-dimensional
A site	Aminoacyl-site
A_{260}	Light absorbance at 260 nanometres (wavelength)
CC	Cross correlation
Cryo-EM	Cryo-electron microscopy
CSPD	Disodium 3-(4-methoxyspiro {1,2-dioxetane-3,2´-(5'chloro)tricyclo [3.3.1.13,7] decan}-4-yl)phenyl phosphate
CTF	Contrast transfer function
Δ*abcD*	Delta, signifying deletion of gene *abcD*
ΔCC	Difference in cross correlation value.
DIG	Digoxygenin
DNase	Deoxyribonuclease
E. coli	*Escherichia coli*
EDTA	Ethylenediaminetetraacetic acid
EM	Electron Microscopy
EMAN	Electron Micrograph Analysis
EMDB	Electron Microscopy DataBank
Era	*E. coli* ras-like protein
FEG	Field emission gun
FPLC	Fast protein liquid chromatography
FSC	Fourier shell correlation
GTPase	Guanosine triphosphate hydrolase
h1-h45	Helices 1 to 45 of the 30S subunit
IF	Initiation factor
JEOL	Japan Electron Optics Laboratory
Kan^R	Kanamycin resistance
KsgA	Kasugamycin resistance protein
LB	Luria-Bertani
ML	Maximum Likelihood
mRNA	Messenger RNA
N-terminal	Amino-terminal
OD_{600}	Optical Density of light wavelength 600 nm
P site	Peptidyl-transfer site
PAGE	Polyacrylamide gel electrophoresis
PCR	Polymerase Chain Reaction
PRC	Photosynthetic Reaction Centre
PDB	Protein DataBank
RbfA	Ribosome binding factor A
RimM	Ribosome maturation factor M
RNA	Ribonucleic acid

RNase	Ribonuclease
r-protein	Ribosomal protein
rRNA	Ribosomal RNA
RsgA	Ribosome stimulated GTPase A
RT	Room temperature
S1-S21	Small ribosomal proteins 1 to 21
SC	Supervised Classification
SPIDER	System for processing image data from electron microscopy and related fields
SSC	Saline sodium citrate
TBE	Tris borate EDTA
TEM	Transmission electron microscope
tRNA	Transfer RNA
UCSF	University of California, San Francisco
WT	Wild type
Xmipp	X-window-based Microscopy Image Processing Package

Contributors to this thesis

All experiments presented in the results section of this thesis were conducted by myself, with the exception of cryo-EM image acquisition. Ahmad Jomaa, Ph.D. candidate, prepared the holey carbon grids, performed sample vitrification, acquired the micrographs, and developed the resulting negatives.

1. INTRODUCTION

1.1 Structure of the bacterial ribosome

The bacterial ribosome is a 2.5 mega-Dalton complex composed of three strands of ribosomal RNA (rRNA), and over fifty ribosomal proteins (r-proteins) bound to the larger nucleic acid complex. Two subunits associate to form the functional ribosome. The large subunit, or 50S, is composed of two rRNAs (5S and 23S) and 33 r-proteins, and contains the catalytic centre that forms the peptide bonds of polypeptides, as well as the space where the nascent protein is extruded during translation (Ban et al. 2000). The small subunit, or 30S, is responsible for binding the messenger RNA (mRNA) and mediating and monitoring the interaction between the message codons and the cognate transfer RNA (tRNA) anticodon at the decoding centre. The 30S contains one rRNA, the 16S strand, and 21 r-proteins (Wilson and Nierhaus 2007; Wimberly et al. 2000). The subunit is further defined into domains based on the rRNA secondary structure, termed the 5' major domain, central domain, 3' major domain, and 3' minor domain, respectively. The terms Head, Platform, and Body define large morphological regions of the subunit, seen in Figure 1. The 16S rRNA is folded into more than 50 helices, which arrange to form the tertiary rRNA structure that makes up the bulk of the 30S subunit and upon which the 21 r-proteins bind. Helix 44 (h44), indicated in Figure 1, forms the decoding centre at its 5' end and contains the functionally essential, conserved adenine residues (A1492 and A1493) required for translational fidelity (Wimberly et al. 2000).

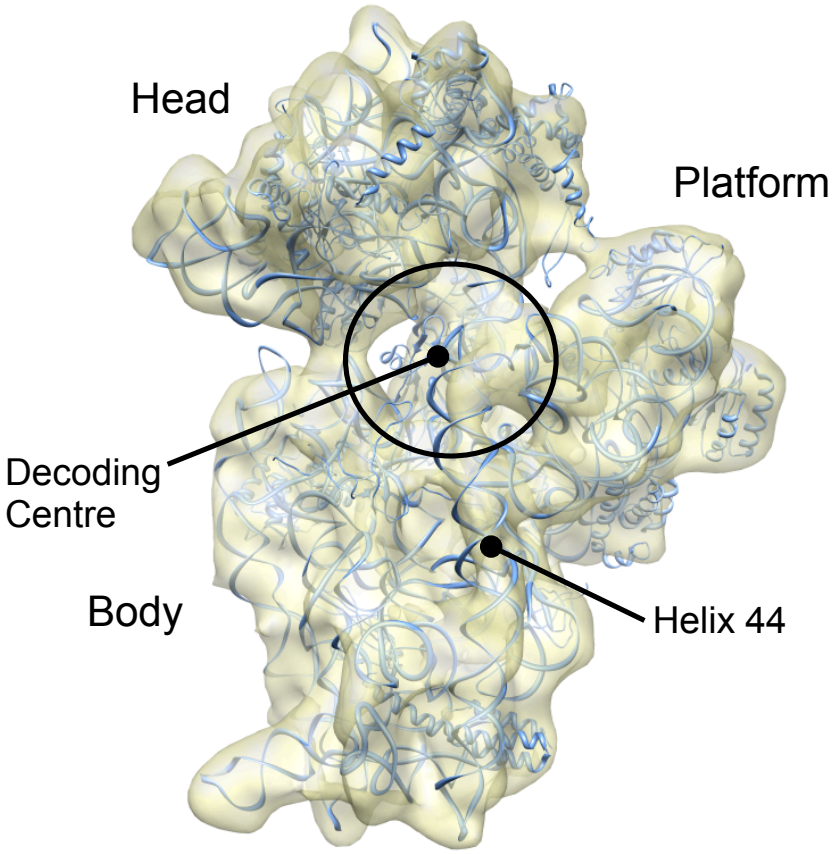

Figure 1: The *E. coli* 30S subunit. The small subunit, here viewed from the interface side, is the portion of the ribosome responsible for mRNA binding and codon:anticodon matching at the decoding centre, indicated by the circle. The structure largely consists of a single rRNA molecule that has a four-domain fold forming the landmarks of the structure: the body (5' domain), the platform (central domain), the head (3' major domain) and helix 44 (3' minor domain). Twenty-one ribosomal proteins bind to the rRNA structure. (Figure prepared in USCF Chimera, with EMDB 1775 and PDBID 2AVY.)

1.2 Assembly of the 30S subunit

A large part of the current understanding of 30S subunit assembly is based upon *in vitro* observations. Reconstitution experiments pioneered by Nomura and colleagues demonstrated that functional 30S subunits of *Escherichia coli* can be generated from purified 16S RNA and r-proteins. This self-assembly demonstrates that the information

necessary for successful subunit formation is contained in the components themselves (Traub and Nomura 1968). Order-of-addition experiments using various combinations of r-proteins revealed that the r-proteins bind to the 16S rRNA in a hierarchical fashion. Some r-proteins bind to the rRNA directly, while some require other proteins to be bound first, which is summarized in the Nomura assembly map (Held et al. 1974; Mizushima and Nomura 1970). This map has since been refined to include new information on the map position of S13 (Grondek and Culver 2004), as reproduced in Figure 2. However, *in vitro* reconstitution of 30S ribosomal subunits involves non-physiological buffer conditions, and low temperatures combined with a heating step to advance the process beyond a stalled reconstitution intermediate. *In vitro* assembly also takes considerably more time than is practical in a living cell, and begins with processed 16S rRNA (Holmes and Culver 2004; Traub and Nomura 1968).

In contrast, the bacterial ribosome assembly process *in vivo* can produce a fully mature 70S ribosome in less than three minutes at 37°C (Champney 1977) and the protein binding and rRNA folding begin as the rRNA is transcribed (de Narvaez and Schaup 1979). In the cell, all three ribosomal RNAs are first produced as part of a single transcript that is processed by ribonuclease (RNase) III cleavage into precursor forms of the 5S, 23S, and 16S strands (Srivastava and Schlessinger 1990). Pre-16S rRNA, or 17S, is bound by r-proteins and undergoes further processing by two endoribonucleases, RNases E and G, to remove 115 nucleotides from the 5' end of the transcript, while an unknown RNase removes 33 nucleotides from the 3' end (Li et al. 1999). Though the ribosome may self-assemble in controlled *in vitro* conditions, ribosome maturation in

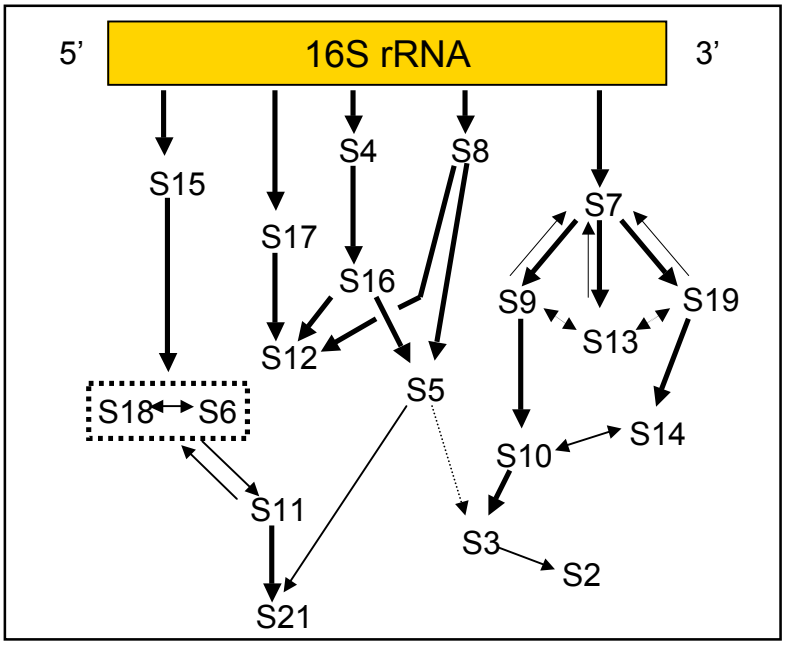

Figure 2: The Nomura 30S subunit assembly map. Seminal reconstitution studies by the Nomura group revealed a binding hierarchy among r-proteins associating with the 16S rRNA. Primary binding proteins, such as S7, can bind naked rRNA, while secondary proteins such as S19 require at least one primary protein to bind first. Tertiary proteins such as S10 require at least one secondary and one primary protein to be bound before its incorporation. Arrow weight indicates strength of dependency. The dashed box indicates r-proteins bound to one another. Figure reproduced from Grondek et al. 2004.

the cell is facilitated by a range of non-ribosomal protein factors, in addition to RNases (Wilson and Nierhaus 2007).

Early pulse-labelling experiments revealed at least two assembly intermediates of the 30S subunit *in vivo* that contain pre-16S rRNA. These are in low proportion compared to mature subunits in the rapidly growing cell and do not entirely correspond to the reconstitution intermediates observed *in vitro* (Lindahl 1975; Maguire 2009; Shajani et al. 2011). Pulse-chase quantitative mass spectrometry experiments confirm earlier observations that the reconstitution intermediates formed at low temperatures *in vitro*

have a variable composition and do not represent a single, defined intermediate particle (Talkington et al. 2005). 30S subunit assembly is likely a multi-step process that occurs via coincident local binding and conformational changes, rather than a step-by-step procession of global structural events (Talkington et al. 2005). A study by the Williamson group investigated the structural features of assembling 30S subunits *in vitro,* using negative stain electron microscopy (EM) and reference-free classification to discover and classify groups of maturing subunits at different time points during an assembly reaction. The experiments revealed support for the parallel assembly models, as variable intermediates were observed that were incorporated into an overall population shift toward the mature state corresponding to various protein binding rates (Mulder et al. 2010).

The application of the insights gained from reconstitution experiments to the assembly of the 30S subunit *in vivo* is complicated by the fact that the mature 16S transcript is used in reconstitutions. This approach limits any insight into the influence of co-transcription and rRNA processing on the assembly of the 30S, as well as the role of several assembly cofactors and chaperones identified *in vivo* (Connolly and Culver 2009; Wilson and Nierhaus 2007). In the EM study by Mulder et al., some kinetically trapped populations were observed during reconstitution that had bound r-protein S2 in advance of its usual antecedent S3 (Figure 2), and assembly therefore was limited by the slow binding of S3 out of its usual order (Mulder et al. 2010). As well, some “dead end” intermediates were observed that showed poorly formed platform and spur regions and did not appear to progress toward maturity. Based on this and other evidence summarized

in that study, they proposed that the function of non-ribosomal assembly factors *in vivo* could be to minimize the formation of trapped intermediates (Mulder et al. 2010). It seems plausible that related assembly factors function together to favour and facilitate particular assembly pathways over others in the complex assembly landscape. However, as the maturing subunit assumes an increasingly mature conformation, fewer pathways present themselves and the precise interplay of the late assembly factors like RimM, RbfA and YjeQ becomes more subtle, with redundancies and as-yet-unrevealed co-operations complicating the interpretation of biochemical data.

1.3 Cofactors involved in late 30S subunit assembly

Genetic and biochemical data have implied a role for many protein factors in the assembly of the bacterial ribosome. In addition to the processing RNases, 30S assembly involves the actions of at least two GTPases, RNA and protein modification enzymes, and other chaperones (Connolly and Culver 2009;Wilson and Nierhaus 2007). These factors include the methyltransferase KsgA (Connolly et al. 2008); a cold-shock factor, RbfA (Bylund et al. 1998; Datta et al. 2007; Inoue et al. 2006); and GTPases such as Era (*E. coli* ras-like protein), which is an essential cellular enzyme (Inoue et al. 2006), and YjeQ/RsgA, another GTPase associated with late 30S subunit biogenesis (Daigle and Brown 2004; Goto et al. 2011; Hase et al. 2009; Jomaa et al. 2011a; Jomaa et al. 2011b). These assembly factors have been genetically and functionally linked to each other and to the protein of particular interest to this work, ribosome maturation factor M (RimM),

through the aforementioned research and wider study of protein interactions (Campbell and Brown 2008).

KsgA is a methyltransferase that is universally conserved (O'Farrell et al. 2006). KsgA dimethylates adenosines 1518 and 1519 located in a loop of in helix 45, near the 3' end of the 16S rRNA (Helser et al. 1972; Poldermans et al. 1979). When KsgA is deleted in *E. coli*, the bacteria exhibit a cold-sensitive growth defect that is indicative of ribosome assembly disruption (Connolly et al. 2008). In addition, Δ*ksgA* accumulates the 17S precursor rRNA and shows disruption in the proportion of free ribosomal subunits relative to active 70S at sensitizing temperatures as assessed by ribosome sedimentation profiles in sucrose gradients. It is a late-acting assembly factor that appears to perform its methylation step before the 17S rRNA is processed (Connolly et al. 2008).

Ribosome biogenesis factor A (RbfA) is similarly implicated in late 30S subunit biogenesis (Bylund et al. 1998). RbfA associates with the 30S subunit at the tRNA A and P sites and shows a deletion phenotype that includes accumulation of 17S rRNA and an altered ribosome profile (Bylund et al. 1998; Datta et al. 2007; Inoue et al. 2006). The exact function of RbfA in 30S assembly remains unclear; it is hypothesized to facilitate maturation of the 16S rRNA at the 5' end and the 3' end of the 17S rRNA (Bylund et al. 1998; Goto et al. 2011; Xia et al. 2003).

Era, or *E. coli* ras-like protein, is an essential GTPase that interacts with the 30S and may act as a chaperone of rRNA conformation (Sharma et al. 2005). This enzyme has been functionally and genetically linked to other assembly factors, particularly RbfA (Inoue et al. 2006). Depletion of Era results in inefficient maturation of 17S rRNA and a

reduced proportion of 70S ribosomes relative to free subunits, similar to Δ*rbfA*. Over-expression of KsgA can suppress a mutation of Era (Lu and Inouye 1998), while over-expression of Era can complement Δ*yjeQ* (Campbell and Brown 2008) and Δ*rbfA* (Inoue et al. 2003).

Another GTPase, YjeQ (also known as RsgA), is linked to the factors described above in facilitating rRNA maturation. When it is deleted, the Δ*yjeQ* strain has a very similar phenotype to Δ*rbfA*, with loss of polysomes and a higher proportion of free ribosomal subunits (Daigle et al. 2002;Daigle and Brown 2004;Hase et al. 2009;Himeno et al. 2004). YjeQ promotes release of RbfA from the 30S subunit during late assembly in a GTP-dependent manner (Goto et al. 2011). Over-expression of Era partially complements the Δ*yjeQ* phenotype, while over-expression of KsgA exacerbates the defects (Campbell and Brown 2008).

1.3.1 Ribosome Maturation Factor M

Ribosome maturation factor M (RimM) is a 21-kDa protein involved in late small subunit assembly of the bacterial ribosome, and is necessary for efficient 16S rRNA processing and 30S subunit maturation (Bylund et al. 1998). Specifically, it has been shown to bind to r-protein S19, which is situated in the head region of the 30S (Lovgren et al. 2004).

Deletion of *rimM* produces a slow, cold-sensitive growth phenotype in *E. coli,* lowered stationary cell density, reduced translation efficiency, and an accumulation of immature 17S rRNA (Bylund et al. 1997; Bylund et al. 1998). Like the other factors

whose disruption results in inefficient rRNA maturation, RimM does not appear to be the RNase responsible for cleavage of the 3' end (Lovgren et al. 2004). Polysome populations, 70S ribosomes, and the amount of 30S relative to 50S are reduced compared to wild type (Lovgren et al. 2004). Mutations in r-protein S13 and increased expression of RbfA can suppress these phenotypes; however, over-expression of RimM does not complement *rbfA* deletion (Bylund et al. 1998; Shajani et al. 2011).

RimM is well conserved among bacteria and has two distinct, ß-strand-rich domains joined by a loop (Suzuki et al. 2007) (Figure 3). The N-terminal domain is a ß-barrel structure and contains a GXXG motif common to KH (K homology) domains, which bind RNA (Bylund et al. 1997; Grishin 2001). KH domains are found in both RbfA and Era. A binding function or other contribution of this domain in RimM has yet to be conclusively demonstrated, though NMR results suggest that a hydrophobic patch on the bottom of the domain may interact with S19 (Suzuki et al. 2007). The C-terminal domain consists of a Photo Reaction Centre ß-barrel (PRC-barrel) motif, first described in the H subunit of the photosynthetic reaction centre in purple bacteria, where it is involved in mediating electron transfer during photosynthesis and protein-protein interactions in the PRC complex. The PRC-barrel found in RimM lacks an acidic residue related to redox regulation, and likely functions as a structural chaperone in 30S subunit assembly (Anantharaman and Aravind 2002).

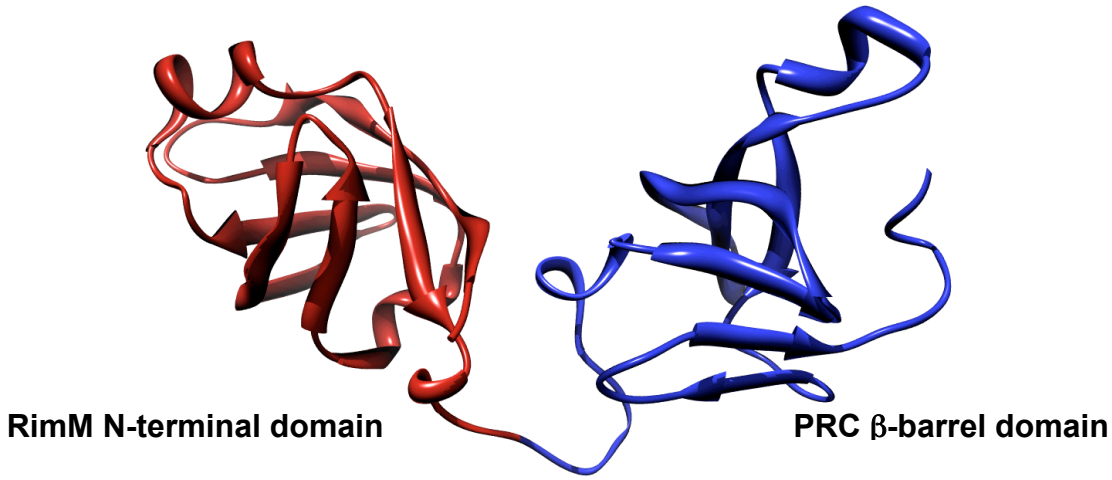

Figure 3: Ribosome maturation factor M (RimM). A 21-kDa, two-domain protein involved in 30S subunit assembly. The N-terminal domain contains a KH-like motif which may be involved in RNA binding, while the PRC barrel domain interacts with ribosomal protein S19, located at the head of the small subunit (Lovgren et al. 2004). Figure prepared from PDB ID 2DYI using USCF Chimera.

Two conserved tyrosine residues located in the linking loop near the PRC-barrel domain of RimM were shown to be essential for interaction with r-protein S19 (Lovgren et al. 2004). Lovgren and colleagues obtained results in pull-down assays that show that RimM binds to subunits containing processed 16S rRNA; however, they did not capture substantial amounts of 17S-containing subunits (Lovgren et al. 2004). An earlier study reported RimM associates with free 30S subunits, but not with 70S ribosomes, and not with 30S subunits that have been in 70S ribosomes, based on pelleting assays (Bylund et al. 1997).

A crystal structure of *Thermus thermophilus* RimM bound to S19 was deposited in 2009 to the Protein Data Bank by Kaminishi et al. (PDB ID: 3A1P). The model suggests that the PRC-barrel forms multiple binding contacts with a ß-sheet region of the

S19 globular domain as well as with the extended C-terminal tail. In this conformation, the RimM N-terminal domain may extend into the A site when RimM is bound to the 30S via S19, and may have a role in the formation of the decoding centre. However, the proteins are bound together in isolation from the 30S subunit, and RimM has not been shown to bind to free r-proteins *in vivo* (Lovgren et al. 2004), thus the structure of the complex may not represent the conformation *in vivo*.

It has been observed that binding of S19 to the rRNA is necessary for a conformational change during 30S assembly *in vitro* (Holmes and Culver 2004), and that addition of RimM to reconstitution mixtures increases the binding rate of S19 (Bunner et al. 2010a). Additionally, binding of S19 along with S7 increases the binding rates of all head r-proteins (Bunner et al. 2010a). A prevailing hypothesis is that RimM may facilitate 30S maturation by mediation of S19 binding and protein interaction in the assembling head region (Lovgren et al. 2004), in addition to possible interactions with other factors.

Addition of recombinant, purified assembly factors to 30S subunit reconstitution reactions has been shown to affect assembly *in vitro*. Three factors, including Era and RimM, increased binding rates of certain r-proteins, and/or inhibited the efficient inclusion of others, possibly due to steric hindrance by bound accessory factors (Bunner et al. 2010b). RimM accelerated binding of S19 to the 30S subunit while retarding addition of S13, suggesting the latter protein may be physically blocked by the presence of RimM on the assembling head.

The complementary effects of related assembly factors cannot be overlooked when attempting to understand the true effects of assembly factors. As noted, a common phenotype among some assembly factor deletions is improper or inefficient rRNA maturation (Bylund et al. 1998; Connolly et al. 2008; Himeno et al. 2004; Jomaa et al. 2011a), and the addition of single assembly factors to reconstitution reactions containing mature 16S rRNA cannot shed light on the role of these assembly proteins in rRNA maturation, or on the significance and timing of rRNA maturation in 30S assembly. Without further data on the precise structural and biochemical interactions of assembly factor proteins, it is difficult to create a model of factor-mediated assembly *in vivo* (Connolly and Culver 2009). Capture of *in vivo* intermediates is complicated by the rapid flux in small populations of immature subunits in wild type *E. coli*. Assembly-factor deletions offer a useful tool for slowing the process so that a "snapshot" of earlier stages of 30S subunit construction can be obtained.

1.4 Structural studies of factor-mediated assembly

Cryo-EM data obtained by Jomaa et al. show that a *yjeQ* deletion mutant accumulates immature 30S subunits containing 17S rRNA, with a severely deformed decoding centre (due to displacement of helix 44) and underrepresented r-proteins such as S2 and S21 (Jomaa et al. 2011a). Based on this information, it seems that proper maturation of the 3' end of the rRNA is essential for functionality; the 3' terminal helices 44 and 45 cannot gain their mature conformation and h44 is not in a position to monitor interaction between the mRNA and tRNA. Indeed, the malformation of the essential helix

also seems to leave the immature 30S incapable of associating into 70S ribosomes at all, as key contact points of helix 44 to the 50S are disrupted (Jomaa et al. 2011a). Thus, the functional deficiencies observed in biochemical studies of YjeQ knockouts are readily correlated with structural data.

A co-structure of YjeQ with the 30S subunit published by Jomaa et al. shows that YjeQ binds on the interface side of the 30S and interacts with helix 44 as well as with the head and the platform of the subunit (Jomaa et al. 2011b). This position suggests that YjeQ, along with other assembly factors, acts as a chaperone to correctly position these domains relative to each other and to facilitate maturation of the 3' end of the rRNA. In addition, YjeQ may help to exclude initiation factors and block bridge contacts with the 50S, preventing an immature 30S subunit from entering into the translation machinery (Jomaa et al. 2011b). Another model of the YjeQ:30S complex also shows that binding of YjeQ would block initiation factors, and that it interacts with h44. However, differences between this model and the one by Jomaa et al. lead to a differing interpretation of YjeQ domain positions and model for interactions (or binding conflict) with other assembly factors known to bind nearby (Guo et al. 2011; Jomaa et al. 2011b). Both studies propose that the structural basis for YjeQ promotion of RbfA release is a YjeQ-induced conformational change in h44 that changes the interaction of the helix with RbfA (Guo et al. 2011; Jomaa et al. 2011b).

RbfA binds to the 30S subunit deep in the junction of the head and body, interacting with helix 44, extending toward helix 1, and interacting with S13 (Datta et al. 2007). When bound to the 30S, RbfA alters the position of the 3' helices 44 and 45 (Datta

et al. 2007), and may position those structures for processing to the mature state and/or interaction with other factors such as YjeQ. In addition, the contact between the C-terminal tail of RbfA with helix 1 may facilitate 5' maturation either in the RNase processing stages or by assisting the cleaved end to gain a mature conformation (Dammel and Noller 1995; Datta et al. 2007).

The proposed function of YjeQ as a release factor for RbfA may be the reason for their similar knockout phenotypes (i.e. accumulation of 17S), as neither case allows progress beyond the RbfA substrate particle. This hypothesis would be supported if a Δ*rbfA* 30S subunit proved to be strikingly similar to the Δ*yjeQ* 30S model solved by Jomaa et al. Goto and colleagues conclude that YjeQ does not associate with 17S-containing pre-30S subunits, and therefore propose a model in which RbfA binds, the rRNA is cleaved to mature 16S, and then YjeQ arrives to dissociate RbfA (Goto et al. 2011). This scenario is inconsistent with the observation that deletion of YjeQ results in accumulation of 17S rRNA (Jomaa et al. 2011b), since in this case RbfA would facilitate normal maturation and the ribosome defect would be due to RbfA's slow dissociation from the 30S subunit and blocking of association with 50S. The biochemical data obtained by Goto et al. is from *in vitro* experiments, without the interplay between various assembly factors.

Era appears to be the chaperone of a more global conformation in the assembling 30S subunit. Era binds between the head and the platform of the 30S, where it makes contact with the central domain and both 3' domains of the 16S rRNA, including helix 45, and with r-proteins S7, S11, and S18, among other components (Sharma et al. 2005). The

subunit has an altered conformation in the Era-bound state, with the head bent toward the platform, and the 50S will not bind to the 30S when Era is bound. The nucleotides with which Era makes contact are adjacent to the anti-Shine Delgarno sequence. This region is highly conserved and required for association of the 30S with mRNA and fMet-tRNA and the initiation of translation. Era likely also excludes S1, a protein involved in interaction between the anti-Shine Delgarno sequence and the mRNA (Sharma et al. 2005). Thus, when bound, Era also prevents entry of the 30S into translating 70S ribosomes.

The most recent publication describing an assembly factor-30S co-structure shows that the methyltransferase KsgA binds on the interface of the 30S somewhat below the platform and contacting helix 45 (Boehringer et al. 2012). Helix 44 appears entirely excluded from its position along the interface, and is not visible in the reconstruction, while h45 remains mostly in place. The flexible orientation is seen in both the co-structure and the KsgA-free model reconstructed from Δ*ksgA* 30S subunits (Boehringer et al. 2012). Bound KsgA alters the decoding centre by blocking interaction between helices 44 and 45. KsgA, along with related factors, may contribute to a conformation of the 3' end of 17S rRNA that is available for RNase processing.

These studies indicate an interrelationship between assembly factors that includes both coincident actions in late assembly and a possible binding hierarchy similar to that of the r-proteins. YjeQ seems to promote release of RbfA during late assembly (Goto et al. 2011), yet RbfA appears to remain bound to 30S subunits in a *rimM* deletion strain as well (Bunner et al. 2010a), indicating that in the absence of RimM YjeQ is either less

efficient or unable to facilitate the complete dissociation of RbfA. It is possible that RimM also facilitates RbfA release, or that it dissociates in tandem with RbfA. Boehringer et al. argue that since the binding of RbfA displaces helix 45 from the platform, RbfA is released (by YjeQ) before KsgA associates with the 30S and methylates helix 45 (Boehringer et al. 2012). Some factors such as RbfA and Era, appear to induce conformations that would not allow simultaneous binding (Datta et al. 2007; Guo et al. 2011; Sharma et al. 2005).

While fully reconciling the various models is difficult at present, it is nonetheless clear that investigation of the structures of *in vivo* assembled immature 30S subunits and co-structures of the 30S with late-acting maturation factors offers a wealth of information upon which to build a complete model of this stage of 30S subunit biogenesis. There is encouraging similarity between the Δ*ksgA* 30S and the KsgA:30S co-structure (Boehringer et al. 2012), as well as correspondence between deletion and binding of YjeQ and distortion of h44 (Jomaa et al. 2011a; Jomaa et al. 2011b), which offers evidence for the utility of assembly factor knockouts in investigating 30S biogenesis, particularly with regard to identifying substrates and gaining a clearer idea of the timing of maturation events. Visualization of the consequences of assembly-factor deletion offers an avenue for investigating and explaining the functional roles of the assembly factors, and the significance of particular *in vivo* maturation events in forming the functional 30S subunit. By employing assembly factor knockouts, the proportion of immature subunits among free ribosomal subunits can be enriched for isolation and study.

2. MATERIALS AND METHODS

2.1 Bacterial strains and PCR screening

Escherichia coli BW25113 (EB334), and the Δ*rimM* knockout in that background were provided by Dr. E. Brown from Keio Collection stocks (Baba et al. 2006). Screening of the Δ*rimM* stock for deletion of RimM and the presence of the kanamycin resistance (Kan^R) cassette was performed using PCR. The primers used for the analysis were:

P1 5′ ATTCCGGGGATCCGTCGACC

P2 5′ TGTAGGCTGGAGCTGCTTCG

RimM Rev 5′ TTCGTGGGTGGCTCAGAGTGTTTTC

RimM Fwd 5′ CGGTACGAGACGTTCCTTGATACCA

RimM flanking 1 5′ GCCGTCTTTTACCGTTTATCCGGTG

RimM flanking 2 5′ CAAAGCAGCTTAATCTGTCACGGTG

Primers P1 and P2 are the same as those used in the construction of the Keio knockout library by Baba et al., and amplify the entire kanamycin resistance cassette when it is present (approximately 1.2 kb). The primers RimM Fwd and Rev correspond to sites internal to the *rimM* open reading frame intended to yield a product of 400 bp. The RimM flanking primers correspond to upstream and downstream sequences from the rimM gene respectively, in order to positively identify a product the size of the gene (549 bp + 50 bp) or the cassette inserted into the same region (~1.2 kb +50 bp). Template DNA samples were prepared for both strains from overnight cultures (with kanamycin for Δ*rimM*). Cell pellets from 3 ml overnight culture were resuspended in 45 μl 1x TE buffer

(pH8), 5 µl 10x TNE (Tris-NaCl-EDTA) buffer and 5 µl of 10 mg/ml lysozyme. The resuspension was incubated on ice for 30 min then heated at 65˚C for 10 min. DNA was extracted by adding 50 µl equilibrated phenol-chloroform, and the mixture was centrifuged for 3 min at 10,000 x g at RT. The upper phase was recovered and DNA precipitated by adding and equal volume of ice-cold 100% ethanol. DNA was pelleted by centrifugation at 10,000 x g for 20 min at 4˚C, resuspended in ice-cold 70% ethanol and pelleted by centrifuging at the same speed and temperature for 5 min. The pellets were dried and then resuspended in 100 µl sterile H_2O for use in PCR.

The PCR was performed with the following cycle times and temperatures: 5 minutes melting at 95˚C and 30 cycles of amplification (1 minute melting at 95˚C, 1 minute annealing at 63˚C , 2 minutes elongation at 72˚C), followed by a final 20 minute elongation step at 72˚C . The completed PCR reactions were separated on a 1% agarose gel in Tris acetate EDTA, stained with GelRed® (Biotium) and visualized with a UV transilluminator.

2.2 Growth in liquid and solid media

Bacterial culture for the 15-h growth curve was grown in 1 litre Luria-Bertani (LB) broth at 37˚C with shaking, from an initial 1:100 inoculation of overnight culture (with kanamycin, for Δ*rimM*). Samples were taken at appropriate time intervals of 0.25 to 1 hr and culture density (OD_{600}) was monitored. Cultures for the 12-h growth curves at 37˚C and 25˚C were inoculated from overnight culture at a 1:100 ratio into 50 ml of LB and incubated at the indicated temperature with shaking.

Fifty ml of LB broth was inoculated with 0.5 ml of overnight culture and grown at 37˚C with shaking to an OD_{600} of 0.2. Serial dilutions were made in fresh LB up to 10^{-6} and 5 μL was immediately spotted onto LB agar plates. The plates were incubated at 37˚C or 25˚C until wild type colonies reached approximately 2 mm in diameter, or 18 h at 37˚C and 40 hours at 25˚C. The uppermost spot is the growth from undiluted culture.

2.3 Sucrose gradient ultracentrifugation

Ribosomes from the BW25113 parent and the Δ*rimM* strain were purified, using the sucrose gradient separation method described in Daigle and Brown (Daigle and Brown 2004). One litre of culture for each strain was inoculated with 10 ml of overnight culture and grown to an OD_{600} of 0.2. Cultures were then cooled to 4°C, and each subsequent step was carried out at this temperature. Bacteria were harvested at 5,180 x g for 10 min and the pellets resuspended in Buffer A (20 mM Tris-HCl pH 7.5, 10 mM magnesium acetate, 100 mM NH_4Cl, 0.5 mM EDTA and 3 mM 2-mercaptoethanol) with the addition of Roche Complete Mini protease inhibitor cocktail and DNaseI (Roche). Resuspended cells were then lysed by pressurized extruder or by French Press at 750-1000 psi, in four passes. The cell lysate was centrifuged at 30,000 x g for 40 min to clear cell debris. Clarified lysate (S30 fraction) was layered over a sucrose cushion of equal volume, composed of Buffer B (1.1 M sucrose, 20 mM Tris-HCl pH 7.5, 10 mM magnesium (Mg) acetate, 500mM NH_4Cl, 0.5 mM EDTA and 3 mM 2-mercaptoethanol) and centrifuged for 16 h at 100,000 x g. The ribosome pellet was rinsed and resuspended in Buffer C (10 mM Tris-HCl pH 7.5, 10.5 mM magnesium acetate, 500 mM NH_4Cl, 0.5 mM EDTA and 2 mM 2-mercaptoethanol). The resuspended ribosomes were again

centrifuged at 100,000 x g for 16 h.

The washed ribosome pellet was then resuspended in Buffer E (10 mM Tris-HCL pH 7.5, 10 mM Mg acetate, 60 mM NH_4Cl and 3 mM 2-mercaptoethanol) for associating conditions or in Buffer F (10 mM Tris-HCl pH 8.5, 1.1 mM magnesium acetate, 60 mM NH_4Cl, 0.1 mM EDTA and 2 mM 2-mercaptoethanol) for dissociating conditions. Sixty to eighty A_{260} units of resuspended crude ribosomes were then applied to 34 ml 10-30% (w/v) sucrose gradients prepared with Buffer E or F. The gradients were centrifuged for 16 h at 40,000 x g. Gradients were fractionated using a Brandel fractionator apparatus and an AKTAprime FPLC system (GE Healthcare). The elution profile was monitored by UV absorbance, and fractions corresponding to the 30S subunit peak were collected. The 30S subunits were removed from the sucrose buffer by centrifuge spinning at 100,000 x g for 16 h, after which the pellet was rinsed with, resuspended in Buffer E, and stored at -80°C. Sample concentration was determined by sample absorbance at 260 nm, where 1 A_{260} unit is equivalent to 69 pmol of 30S.

The proportion of free 30S to bound 30S (i.e. 30S subunits in 70S binary complexes) is calculated using peak areas of the profiles. The area of the 30S peak plus one-third the area of the 70S peak corresponds to the total 30S population as it contributes to the absorbance. The area of the 30S peak is divided by the total 30S absorbance for the percentage of free 30S.

2.4 Total rRNA isolation and urea-PAGE

Overnight cultures of the parental strain BW25113 and Δ*rimM* knockout were inoculated at a 1:100 dilution into fresh LB media and grown for 15 h at 37°C with shaking. Samples of 2-3 ml each were taken every 30 or 60 minutes. Cells were pelleted in a microcentrifuge at 9,000 x g (all subsequent spins were performed in a

microcentrifuge). Total rRNA from each cell sample was isolated using a Qiagen RNeasy mini isolation kit according to the manufacturer's protocol. Cell pellets resuspended in Buffer RLT (contains guanidine thiocyanate, proprietary detergents, user-added 0.1% v/v ß-mercaptoethanol) were subjected to mechanical lysis using a syringe to force the cell suspension through a 20g needle 15 to 20 times. Lysed cells were centrifuged for 10 s at 9,000 x g to pellet debris, and the supernatant was applied transferred to a clean tube. An equal volume of 70% ethanol was added to the lysate and mixed before the solution was applied to an RNeasy spin filtration column. The lysate was spun through the column at 10,000 rpm for 15 s and the flowthrough discarded. Buffer RW1 (proprietary, contains guanidine salt) was added to the column, and spun through at 8,000 x g and the flowthrough discarded. Buffer RPE (proprietary, with user-added ethanol, total 80% v/v) was applied to the column and the column centrifuged for 15 seconds at 8,000 x g. A second volume of Buffer RPE was applied and spun through for 2 min to fully dry the column membrane. RNA bound to the column membrane was then eluted in 50-100 μl of RNase-free water by centrifuging at full speed (9,000 x g). Sample concentration was then assessed by A_{260}, where 1 absorbance unit is equivalent to 40 μg/ml of RNA.

Samples of 1.5 to 2 μg purified RNA were loaded on an 8 M urea/4% polyacrylamide gel in 1x Tris-borate-EDTA (TBE) assembled in a adjustable slab gel apparatus (CBS Scientific Co.). Samples were separated on the gel at 300V for 16 h, and then stained with ethidium bromide in 0.5x TBE before visualizing on a UV transilluminator.

2.5 Northern blot and detection of rRNA

Total RNA from the parental (wild type) strain, Δ*rimM* and Δ*yjeQ* was purified from cell pellets using a Qiagen RNeasy mini isolation kit as above, and 3-5 μg per

sample was run on an 8 M/4% polyacrylamide gel, also as above. The gel was then washed in 0.5x TBE for half an hour and stained with SYBR® Gold nucleic acid stain (Invitrogen) for UV imaging. Northern blot procedures followed the manufacturer's protocol for the DIG chemiluminescent nucleotide detection (Roche). The gel-separated rRNA was transferred to a nitrocellulose membrane using a Bio-Rad Transblot semi-dry transfer system at 25V for 45 min and fixed by exposing the membrane to UV light (302 nm) for 1.5 minutes. The membranes were equilibrated in Roche Easy-Hyb solution at 50°C for 30 minutes, and then hybridized with 0.1-1 pmol/ml DIG-dUTP-labelled oligonucleotide probes in Easy-Hyb solution and 0.1 mg/ml poly-adenosine at 50°C, overnight. The probe sequences are as follows:

5′ probe - TTAAGAATCCGTATCTTCGAGTGCCCACA

3′ probe - TGTGTGAGCACTGCAAAGTACGCTTCTTTAAGGTAAGG

16S probe - GGGCCATGATGACTTGACGTCATCCCCACC

The hybridized membrane was washed in 2x saline-sodium citrate (SSC) (300mM NaCl, 30mM sodium citrate) once at room temperature (RT), washed twice in 0.5x SSC at 50°C, and once again with 2x SSC at RT. After rinsing with Wash Buffer (100mM maleic acid, 150 mM NaCl pH7.5, 0.3% v/v Tween 20), the membrane was incubated for 30 min at RT in Blocking Buffer (100mM maleic acid, 150 mM NaCl ph 7.5, 1% w/v Roche blocking reagent) after which the Blocking Buffer was discarded. Anti-DIG antibody was added at a 1:10,000 dilution to Blocking Buffer, which was applied to the membrane and incubated at RT for 30 min. The membrane was then washed four times with Washing Buffer before being equilibrated for 5 min in Detection Buffer (100mM

Tris pH 9.5, 100mM NaCl). A 1:100 dilution of CSPD (Roche) in Detection Buffer was then applied to the entire membrane, which was then incubated for 20 min at 37°C, in the dark, to develop the chemiluminescent reaction. Kodak BioMax XAR film was exposed to the membrane and developed to obtain the experimental images. Following hybridization and development with the 3' probe, the probe was stripped from the membrane. The CSPD solution was rinsed from the membrane with distilled water before the membrane was treated with boiling 0.1% SDS for 10 min and then rinsed with Wash Buffer. The probe-stripped membrane was then treated with Roche Easy-Hyb solution and hybridized with the 5' probe, as above. Following a second stripping procedure, the membrane was hybridized a final time with the 16S internal probe.

2.6 Ribosome profiles in early-log, late-log and stationary phase

BW25113 and Δ*rimM* overnight cultures were prepared and inoculated into 1 litre LB broth as above and grown in three separate flasks to OD_{600} 0.2, 0.8 and 3.0—representing early-log, late-log and stationary growth phases of the culture—respectively. Cell pellets were recovered by centrifuge at 5,180 x g for 10 min at 4°C, and then resuspended in Buffer P (10mM Tris pH 7.5, 10mM $MgCl_2$, 60mM KCl) centrifuged a second time at 3,400xg for 15 min, whereupon the buffer was discarded and the pellets flash frozen for storage at -80°C. Thawed cell pellets were then prepared for ribosome purification under associated conditions as described above, excepting that each gradient had a total volume of 11 ml, and was loaded with 10 A_{260} units of washed ribosomes. The gradients were centrifuged at 72,000xg for 14.5 hours. Sucrose gradients

were fractionated and analyzed as above. The experiment was conducted on three separate occasions.

2.7 Negative stain electron microscopy

Copper, 400 mesh electron microscopy grids (Electron Microscopy Sciences) were prepared with a continuous layer of carbon for negative staining. Carbon-coated grids were then glow discharged in air for 30 seconds immediately prior to sample preparation (Aebi and Pollard 1987). 30S subunit samples were diluted to approximately 0.25 or 0.5 μg/ml, and 3 μL of solution was applied to the grids for 2 min, which were then briefly blotted. A 1% w/v uranyl acetate solution was applied to the grids for 2 min, which were then blotted and dried thoroughly. Negative stain images were acquired on JEOL TEMScan at a nominal magnification of 200,000x.

2.8 Cryo-electron microscopy

Copper, 400 mesh electron microscopy grids (Electron Microscopy Sciences) were prepared with holey carbon and an additional continuous thin layer of carbon for cryo-EM. Grids were washed with acetone vapor for 15 min and glow discharged in air for 30 s (Aebi and Pollard 1987). In a Vitrobot (FEI), 3.5 μl aliquots of sample were applied to the grid for 1 min at 25°C and 100% relative humidity. Grids were blotted two times for 7 s and vitrified by rapidly plunging into liquid ethane at -180°C using the Vitrobot (FEI).

The vitrified grids were then transferred to a Gatan 914 side-entry cryo-holder and imaging was performed using a JEOL 2010F FEG microscope at liquid nitrogen temperatures. The microscope was operated under low dose conditions at 200 kV, with a

nominal magnification of 50,000x. In total, 140 micrographs were obtained, with defocus values ranging from 1.4 μm to 3.6 μm. The micrographs were digitized using a Nikon Supercool Scan 9000 with a sampling value of 2.54 Å/pixel. With the exception of the micrograph scanning, the microscopy steps described were undertaken by Ahmad Jomaa, Ph.D. candidate.

2.9 Single particle reconstruction of Δ*rimM* 30S subunit

A total of 59,413 particles were manually picked using EMAN boxer (Ludtke et al. 1999). Micrograph power spectra, CTFs, and information limits were assessed using Bsoft and CTF was corrected in Xmipp using CTFFIND (Mindell and Grigorieff 2003; Scheres et al. 2008). Three-dimensional reconstruction of the Δ*rimM* 30S subunit from a subset of the total images (22,416 particles) was accomplished using Xmipp projection matching (Scheres et al. 2008) using a reference map prepared from the X-ray structure of *E. coli* 30S (PDBID: 2AVY) (Schuwirth et al. 2005) which was low-pass filtered to 25 Å. Angular projections of the reference maps were calculated from 15˚ to 2˚ over the multiple iterations. Resulting reconstructions were masked with a binary mask produced from the reference. Supervised classification (SC) of all particles (Valle et al. 2002) to assess sample heterogeneity employed the X-ray derived reference noted above and initial reconstruction of 22,416 particles as the Δ*rimM* 30S reference (Step 1), resulting in 20,500 particles assigned to the immature class based on differential cross-correlation scores of particle images with projections of both references.

Maximum Likelihood (ML) classification (Scheres et al. 2007a) of the immature particle class (20,500 images) from Step 1 was performed using three initial seeds and the

X-ray structure-derived reference volume low-pass filtered to 70 Å for the initial alignment step (Step 2). Using the least wild-type-like result of ML as the Δ*rimM* reference, a final round of Supervised Classification was performed on all particles, which appeared to improve the SC separation of mature particles versus immature (Step 3). 15,720 particles of the initial dataset were classified as immature in Step 3. These particle images were used in the three-dimensional (3D) reconstruction of the Δ*rimM* 30S subunit. Projection matching was carried out as above, except for the first five iterations. For these rounds of projection matching, a circular mask was used to prevent a reference-based mask from cutting off any protrusions at the interface. After five iterations, a binary mask was generated from the reconstructed volume and applied in the remaining iterations. Resolution of the EM maps was estimated using the Fourier shell correlation (FSC) of two maps calculated from the even- and odd-numbered particles of the last iteration of projection matching. The FSC cutoff used was 0.5.

2.10 Difference mapping

EM maps of the wild type *E. coli* 30S subunit (EMDB #1775) and Δ*rimM* 30S subunit were low pass filtered to the same resolution and normalized such that their average densities and standard deviations were 0 and 1, respectively. Using BSOFT operations, each density map was inverted and then added to the non-inverted map of the other 30S model, resulting in corresponding difference maps of their densities. The *E. coli* 30S crystal structure was fit into the wild type 30S EM map using UCSF Chimera.

3. RESULTS

3.1 Screening and characterization of Δ*rimM* from the Keio collection

PCR analysis of the knockout strain showed that *rimM* was deleted. The gel image in Figure 4 shows the presence of the RimM gene (Lane 2) in the parental strain along with nonspecific bands (Lane 1) arising from the Kan^R cassette primers P1 and P2 (BW25113 is kanamycin sensitive in liquid and solid media, data not shown). In contrast, the P1 and P2 primers amplify at distinct band from Δ*rimM* DNA at approximately 1.2 kb. which is the size of the kanamycin resistance cassette inserted in the Keio collection knockouts (Baba et al. 2006). The RimM primers designed to anneal within the intact gene do not amplify any product. Internal primers were chosen to detect the intact *rimM* gene after primers corresponding to the 5' and 3' ends of the gene amplified large bands in the knockout strain, suggesting that these regions were present flanking the Kan^R insertion site (data not shown). Primers chosen specifically to anneal to *rimM* flanking regions just outside the open reading frame amplify a 600 bp band corresponding to the *rimM* gene (549 bp) and an additional 50 bp added by the primers in the parental strain. In Δ*rimM* a band of over 1.2 kb is amplified by the flanking primers, showing that the gene has been replaced, presumably by the 1.2 kb Kan^R cassette amplified in Lane 4.

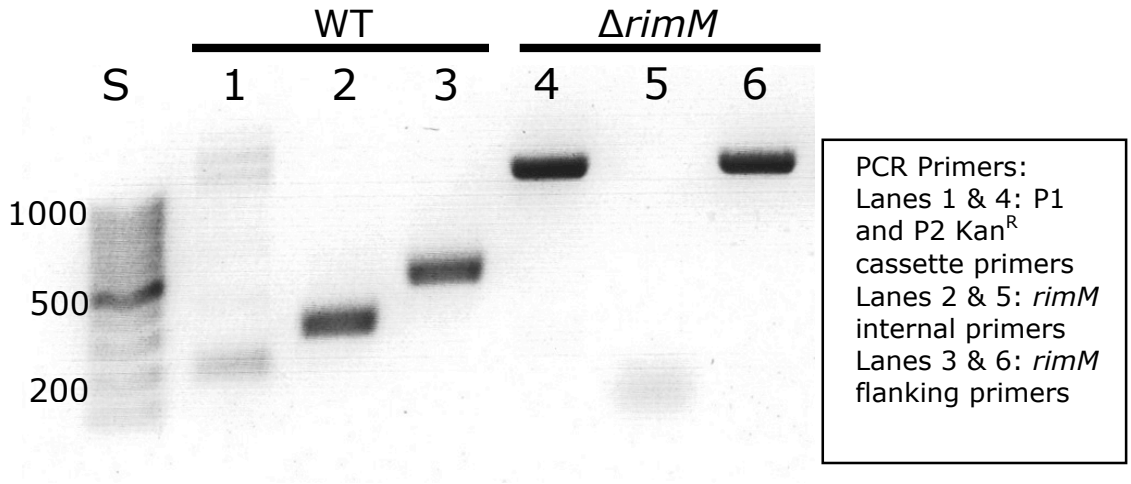

Figure 4: PCR screening confirms deletion of *rimM*. The wild type parental strain BW25113 shows a defined 400 bp product amplified by primers internal to the intact *rimM* gene (Lane 2), and a product of 600 bp corresponding to the complete 549 bp *rimM* gene plus 50 bp in flanking sequences for which the primers were designed (Lane 3). In contrast, the Δ*rimM* strain has a well-defined band of approximately 1.2 kb amplified by primers specific to the Keio collection Kan^R cassette insertion (Baba et al. 2006) (Lane 4), no amplification from primer sites internal to the *rimM* gene (Lane 5), and a large band of slightly more than 1.2 kb, corresponding to a successfully inserted Kan^R cassette flanked by *rimM* extra-gene sequences.

The Δ*rimM* knockout strain has a growth-deficient phenotype, similar to that reported by Bylund et al. (Bylund et al. 1998), when grown in Luria-Bertani medium at 37°C with shaking, and on LB agar in dilution series. RimM is not essential under lab conditions, but it is important for efficient growth in LB. A growth profile collected over fifteen hours at 37°C (Figure 5a) showed that the knockout strain reaches a similar stationary phase density as wild type in LB, and data from three separate growth curves show that the mutant strain typically has 2- to 3-fold slower growth in log-phase than the parental strain (Table 1). Figure 5b shows the growth of both strains at 37˚C and 25˚C.

The growth rates constants of log-phase growth calculated for this particular experiment are 1.39 h^{-1} for wild type and 0.45 h^{-1} for Δ*rimM* at 37˚C, and 0.6 h^{-1} for wild type and 0.21 h^{-1} for Δ*rimM* at 25˚C. The ratio of growth rates at both temperatures is similar, indicating that Δ*rimM* is not much more growth-impaired at 25˚C than the wild type parent. In contrast, culture dilution series on LB agar showed exacerbation of the slow growth phenotype at 25°C; cold sensitivity is a well-known hallmark of ribosome assembly defects in *E. coli* (Connolly et al. 2008) (Figure 5c).

Table 1: Doubling time and growth rate constant of wild type parent and Δ*rimM*

	Doubling Time (DT) (h)	**Growth rate constant (k = ln2/DT) (h^{-1})**
Wild type (BW25113) ***(n=3)***	0.579±0.069	1.207±0.159
Δ*rimM* *(n=3)*	1.417±0.107	0.487±0.04

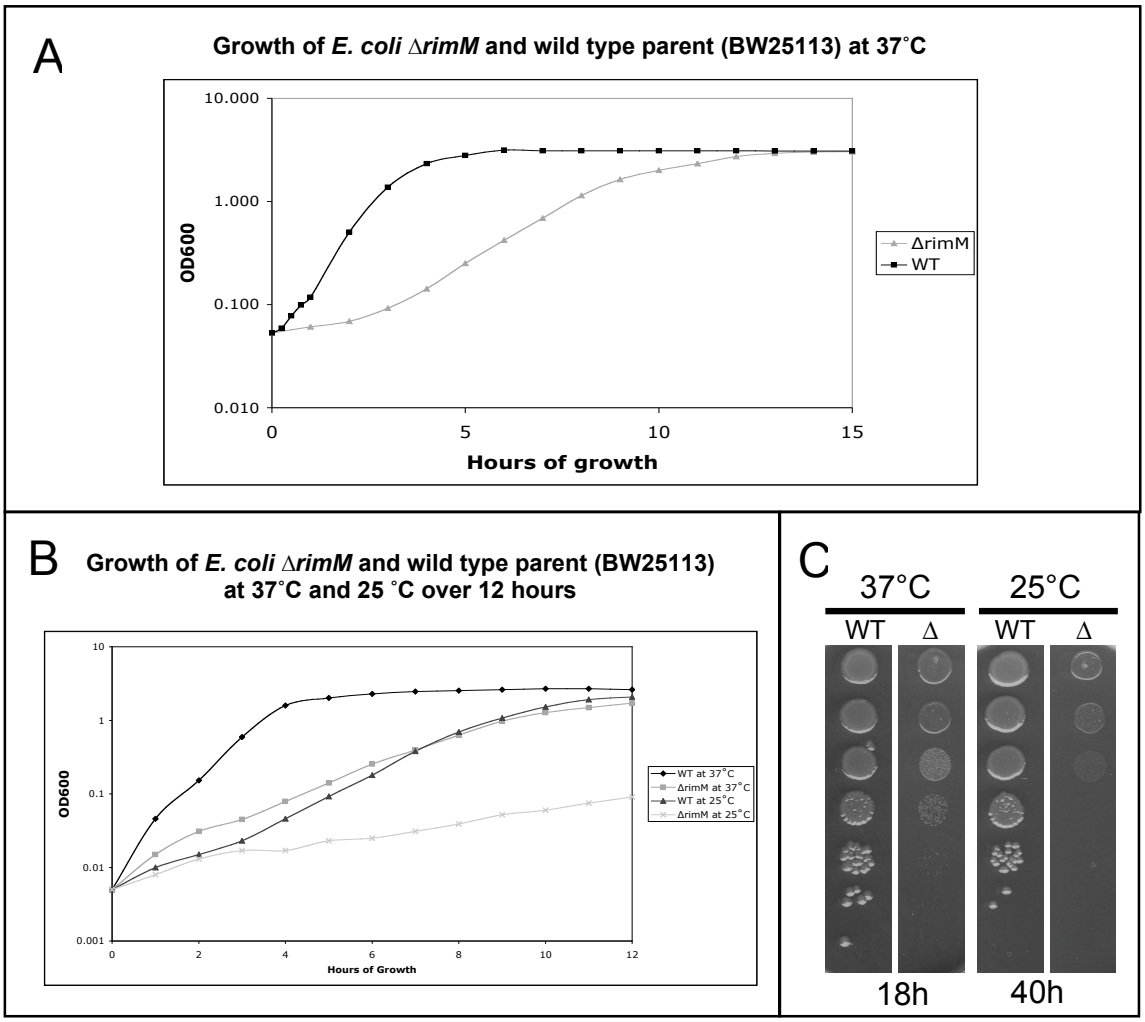

Figure 5: Growth characteristics of Δ*rimM* and parental strain BW25113.
A) Bacterial cultures were grown 1 litre LB broth at 37˚C with shaking. Samples were taken at appropriate time intervals of 0.25 to 1 hour and cell density (OD_{600}) was monitored. RimM deletion results in a log-phase growth deficiency of approximately 2.5-fold compared to the parental strain BW25113 (Table 1) **B)** Δ*rimM* and parental *E. coli* grown in 50 ml LB show a similar growth differential at 37˚C and at 25˚C. **C)** 50 ml of LB broth was inoculated with 0.5 ml overnight culture and grown at 37˚C with shaking to an OD_{600} of 0.2. Serial dilutions were made in fresh LB up to 10^{-5} and 5μL was immediately spotted onto LB agar plates, which were incubated at 37˚C or 25˚C until wild type colonies reached approximately 2mm in diameter, or 18 hours at 37˚C and 40 hours at 25˚C. The uppermost spot is the growth from undiluted culture. Δ*rimM* shows some cold sensitivity relative to growth of wild type. (Dilution series were grown on the same LB plate for each temperature condition; images of spot columns are arranged closer together for the purposes of the figure.)

3.2 16S rRNA maturation is disrupted in Δ*rimM E. coli*

Ribosomal RNA analysis shows that the Keio Δ*rimM* strain has accumulation of a larger small subunit rRNA in addition to 16S, comparable with the Δ*yjeQ* strain which is known to amass 17S rRNA with 115 additional 5' nucleotides and 33 extra nucleotides at 3' (Bylund et al. 1998;Jomaa et al. 2011a;Li et al. 1999).

In order to confirm the identity of the rRNA species accumulated in Δ*rimM*, Northern blot hybridization was performed. Total RNA from the parental (wild type) strain, Δ*rimM* and Δ*yjeQ* was hybridized with DIG-labelled oligonucleotide probes complementary to the 5' end or the 3' end of 17S and a probe corresponding to a short internal region of 16S rRNA, around 1200 nt.

The results of the Northern blot are shown in Figure 6 along with the corresponding polyacrylamide gel (Figure 6b). The 3' probe, complementary to the very end of the additional 33nt of the 17S rRNA (Figure 6a), hybridized with a thick band for both Δ*rimM* and Δ*yjeQ*, and a much less intense band of the same molecular weight in the parental strain (Figure 6c). The probe corresponding to the very terminus of the 5' end hybridizes to the same band detected by the 3' probe, showing that the larger rRNA accumulated in the knockout strains has the incompletely processed ends indicative of the 17S precursor rRNA. The 16S internal probe hybridizes to the 17S band shown by the terminal probes, as well as the smaller mature 16S in the wild type and both knockouts. The band below 16S may correspond to a degradation product of 16S or incorrectly processed rRNA in the knockout strains (indicated by an asterisk, Figure 6c). Its presence is consistent with previous studies of the rRNA content of Δ*yjeQ* strains (Himeno et al.

2004; Jomaa et al. 2011a). These results confirm previous observations that RimM is required for efficient 16S rRNA maturation (Bylund et al. 1998), and that BW25113 Δ*rimM* shows the same deficiency as reported in other strains.

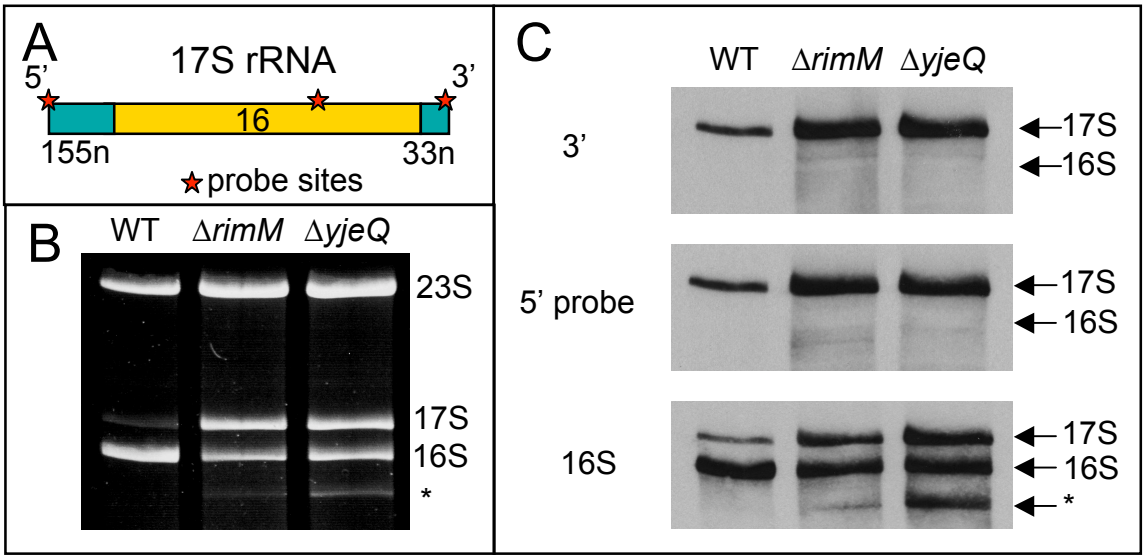

Figure 6: Characterization of Δ*rimM* strain rRNA by gel electrophoresis and northern blot. A) 17S ribosomal RNA has 115 extra nucleotides at its 5' end and 33 extra nucleotides at its 3' end compared to mature 16S rRNA. **B)** Urea-polyacrylamide gel analysis of total rRNA purified from wild type, Δ*rimM* and Δ*yjeQ* (for rRNA size comparison.) Both assembly factor knockouts cause an accumulation of slower migrating rRNA compared to wild type, corresponding to a precursor of 16S likely to be 17S. **C)** The identity of small ribosomal rRNA species is evaluated by northern hybridization using DIG-labelled oligonucleotide probes for chemiluminescent detection. Sequence specific oligonucleotide probes binding to the very 3' or 5' end of 17S, or to an internal site of the 16S rRNA confirm the identity of the accumulated rRNA as 17S. The lower migrating bands indicated by an asterisk indicate an unknown 16S rRNA species, possibly a degradation product.

3.3 Δ*rimM* accumulates free ribosomal subunits

Profound effects on the ribosome content of the Δ*rimM E. coli* accompany the accumulation of 17S rRNA. 30S ribosomal subunits were purified by sucrose gradient ultracentrifugation. Ribosome profiles under 70S-associating (high Mg^{2+}) and 70S-dissociating (low Mg^{2+}) conditions were collected on multiple occasions. Typical profiles for the associated condition are shown in Figure 7. At a culture OD_{600} of 0.2, the Δ*rimM* strain shows an accumulation of free 30S and 50S subunits, and a lower proportion of 70S ribosomes compared to the parental strain. The low availability of functional ribosomes and the energy expended to produce subunits that are then stalled in assembly likely contribute to most of the observed growth defect. Up to approximately 53% of all 30S subunits in the cells are in the free 30S peak and not associated into translating 70S ribosomes, compared to approximately 11% free 30S in wild type *E. coli*.

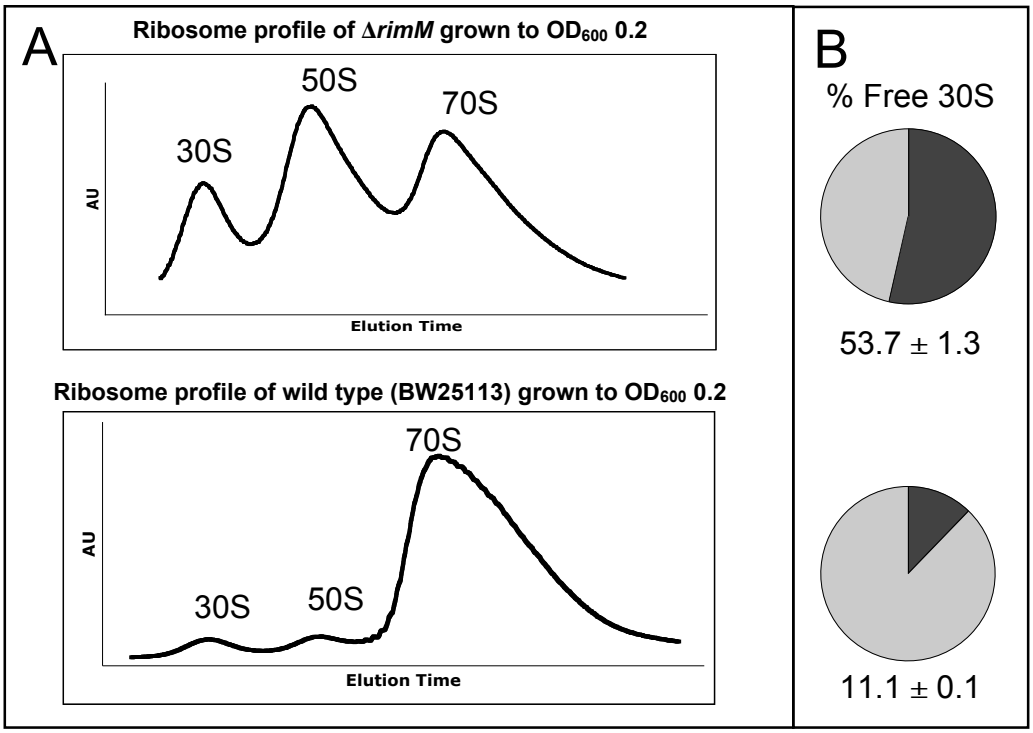

Figure 7: Ribosome distribution in Δ*rimM* and BW25113 at OD_{600} 0.2. Ribosomes from the BW25113 parent and the Δ*rimM* strain were purified on sucrose gradients and fractionated on FPLC. **A)** Δ*rimM* shows a significantly altered ribosome profile compared to its wild type parent, with a notable difference in the proportion of free subunits to 70S ribosomes. **B)** Calculations from the areas under the peaks show for the Δ*rimM* strain the distinct increase (approximately 42%) in the proportion of free 30S subunits (dark grey) relative to those bound in 70S (light grey). (Average ratios calculated from n=5 replicates for Δ*rimM* and n=4 for wild type).

Samples from the Δ*rimM* 30S peak were collected for imaging using negative stain electron microscopy. Images show that such samples consist largely of 30S subunits, with some minimal contamination of 50S subunits and other complexes (Figure 8). Samples from the same purification were used for cryo-EM imaging.

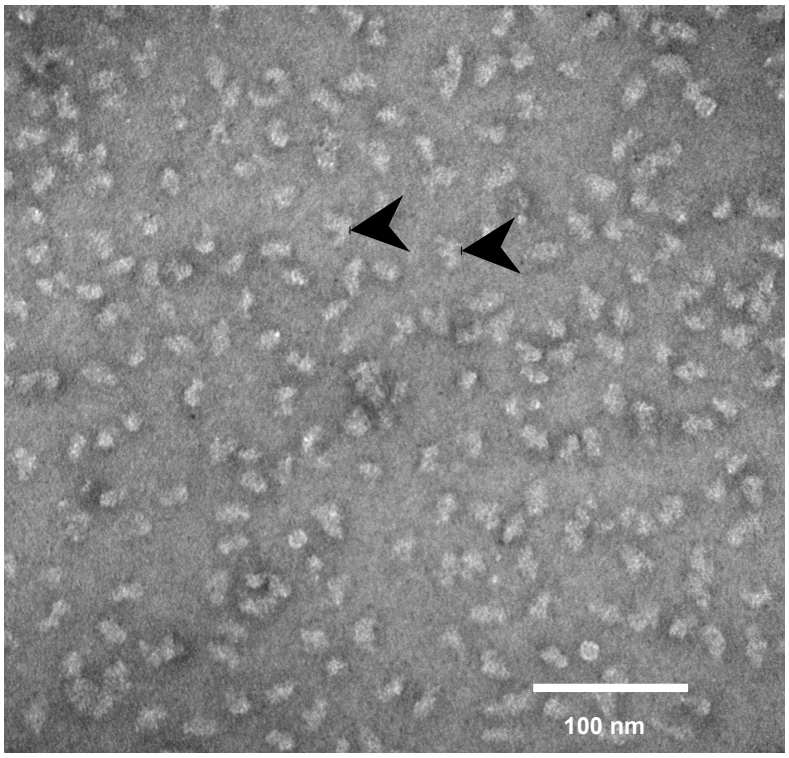

Figure 8: Negative stain electron micrograph of 30S subunits collected from Δ*rimM* at OD_{600} 0.2. 30S subunit samples were applied to 400-mesh copper grids with continuous carbon and stained with 1% w/v uranyl acetate. Images were taken on a TEMScan. This image shows the irregular morphology of 30S subunits (particle indicated by arrowheads). More globular particles indicating the presence of 50S or protein complexes are minimally present in the sample.

3.4 17S rRNA proportions are not stable throughout growth

Other assembly factor knockouts such as Δ*yjeQ* appear to recover their distorted ribosome profiles to more wild type-like states as growth progresses past log phase (Geordie Stewart, unpublished data). To determine if there is any fluctuation in the accumulation of 17S rRNA over the course of growth, the parental strain BW25113 and Δ*rimM* were grown at 37°C and samples were taken at 30 to 60 minute intervals over 15 hours for both strains, corresponding to the growth curve in Figure 5a. Total RNA was

purified from cell pellets using a Qiagen RNeasy mini isolation kit, and run on 4% polyacrylamide/8M urea gels (Figure 9). The quantity of 17S rRNA accumulated in the Δ*rimM* strain remains largely unchanged during log phase growth, but as the culture begins stationary phase at approximately 10 hours, a distinct decrease in 17S rRNA is apparent. The wild type exhibits a stable amount of 16S rRNA relative to 23S (the larger rRNA of the 50S subunit). Small amounts of 17S rRNA can be seen during log phase growth, as well.

The shift from log phase to stationary phase growth is accompanied by less demand for ribosome production, and hence immature rRNA transcripts cease to accumulate as the rate of maturation begins to exceed production. Alternatively or concurrently, the remaining 17S rRNA may be degraded as other ribosome assembly processes are down-regulated.

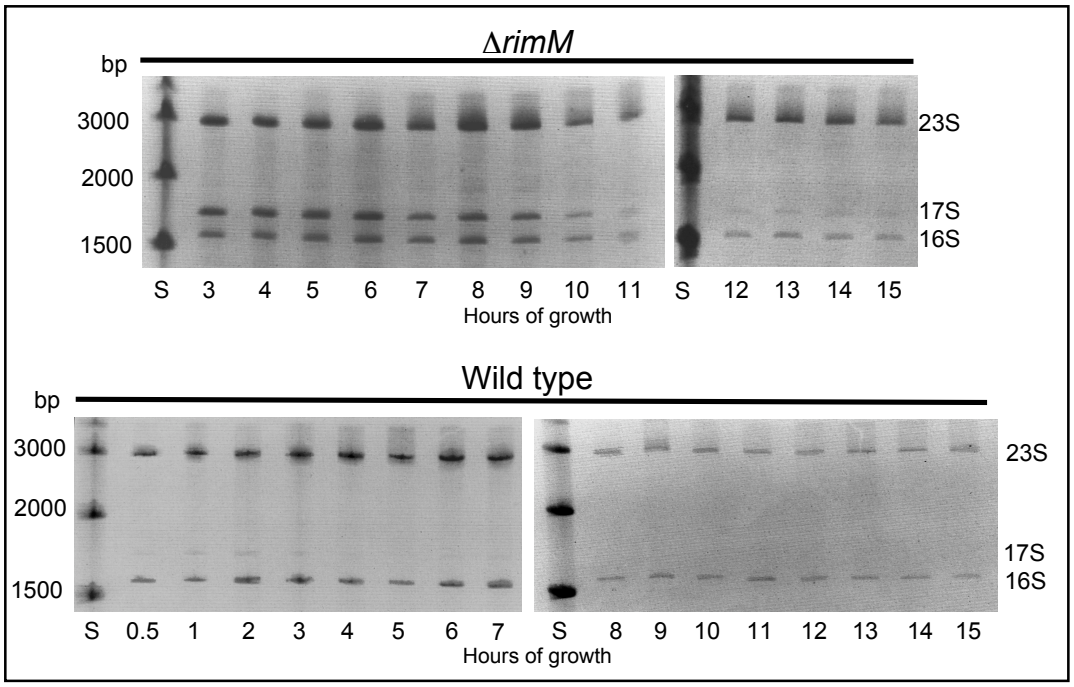

Figure 9: Analysis of rRNA profiles during culture growth at 37˚C. Samples taken during the 15-hour growth curve in Figure 5 were pelleted for total rRNA purification and urea-polyacrylamide gel electrophoresis (hours 1 and 2 represent lag phase and were omitted from the Δ*rimM* gel). Δ*rimM* shows a steady level of 17S rRNA during log-phase growth; however as the culture enters stationary phase at approximately 11 hours, 17S rRNA accumulation drops dramatically while 16S appears mostly unchanged (relative to 23S, used as the loading reference). In contrast, the wild type cells exhibit a very small amount of 17S rRNA during log-phase, and maintain a steady amount of 16S relative to 23S over the course of growth.

3.5 30S subunit populations decrease as culture approaches stationary phase

In order to analyze how the decrease in 17S rRNA affects the ribosome population, sucrose gradient profiles for both the parental strain and Δ*rimM* were analyzed at different stages of culture growth, i.e. early log-phase, late log-phase and stationary phase. The results are presented in Figure 10. In early log-phase growth (OD_{600}

0.2) of the RimM knockout, approximately 47% of all 30S subunits are not associated in 70S ribosomes, presumably as a consequence of inefficient rRNA maturation. Ribosomal subunits containing 17S rRNA appear to be inactive and unable to associate into mature 70S ribosomes (Jomaa et al. 2011a; Wireman and Sypherd 1974). As growth progresses, the proportion of free 30S subunits is reduced to approximately 26% of the total in late-log phase (OD_{600} 0.8), and to approximately 10% in stationary phase (OD_{600} 3.0). This reduction in free 30S is not accompanied by a decrease in free 50S, possibly because the excess free 30S subunits are not associating with available 50S subunits to form 70S ribosomes. The stationary phase profile for the parental strain also showed a disappearance of the free 30S subunit pool and maintenance of the free 50S population, suggesting this effect is not particular to cells with defective ribosome profiles and that the stable 16S rRNA observed in the gels (Figure 9) is located in 70S ribosomes as growth progresses.

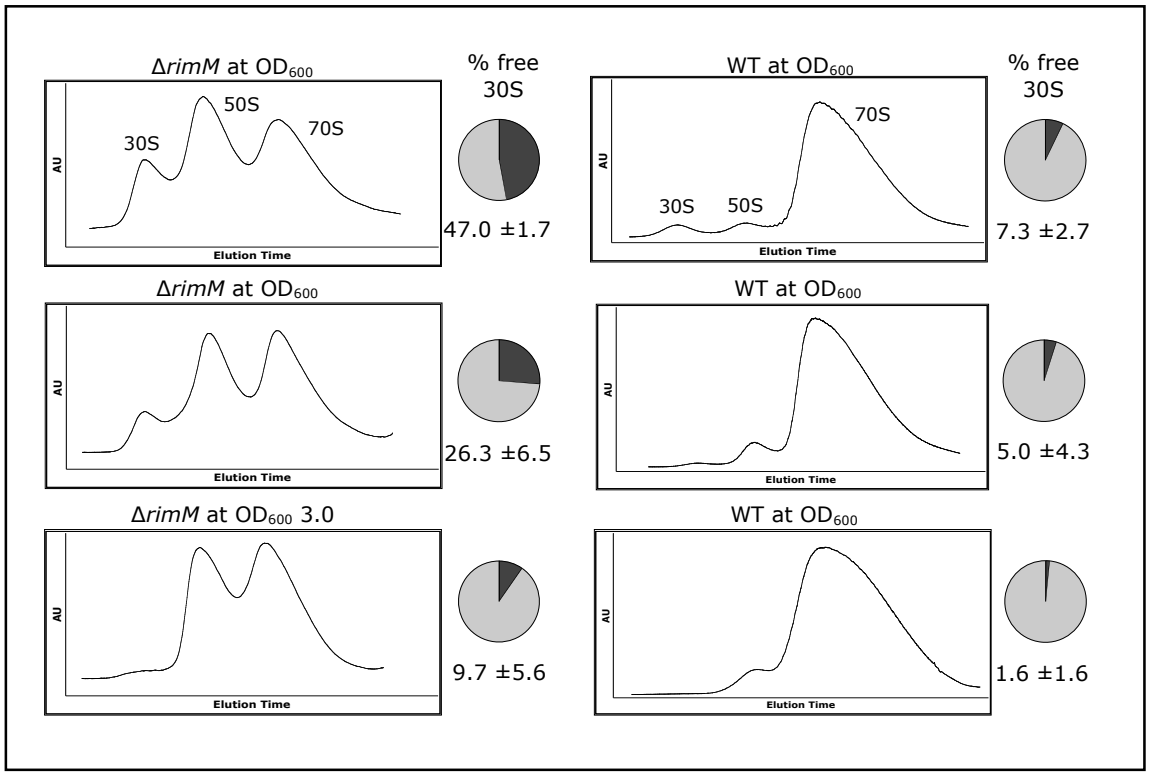

Figure 10: Ribosome profiles and 30S subunit distribution at different culture growth stages. Cell cultures for both strains were grown to an OD600 of 0.2, 0.8 or 3.0 in LB broth at 37˚C with shaking. Ribosome profiles obtained from Δ*rimM* show a pronounced decrease in the proportion of free 30S subunits compared with those bound in 70S (equivalent to a third of the area of the 70S peak), without a corresponding drop on free 50S. A similar decrease of free 30S subunits in wild type profiles was observed as well. This experiment was performed 3 times.

3.6 The Δ*rimM* 30S is a late assembly product with a distorted decoding centre

A 3D model of the 30S subunits accumulated in the RimM knockout was obtained using single particle reconstruction from cryo-EM images. Initial maps showed a subunit that is mostly assembled, with a similar general morphology to wild type, mature 30S, with domains such as the head, platform, and body clearly present (Figure 11).

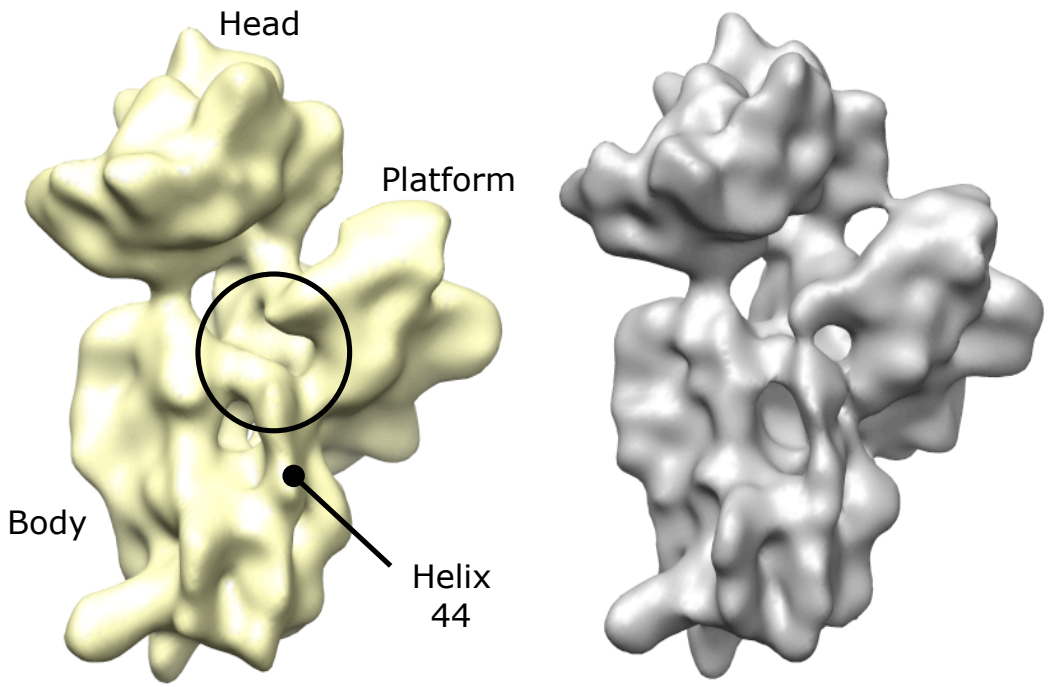

Figure 11: Initial reconstruction of the Δ*rimM* 30S subunit. The average structure from unclassified Δ*rimM* particles (left) shows a similar general morphology to the mature 30S (right) in the regions labelled. However, the Δ*rimM* 30S lacks some density corresponding to helix 44 and the decoding centre, indicated by the leader line and circle, respectively. The map has a resolution of approximately 16Å as calculated by Fourier shell correlation with a cut-off of 0.5. This volume was used in the first round of Supervised Classification (Step 1) as the immature reference. See Figure 12 for supervised classification results. The wild type map was prepared from EMDB 1775, low-pass filtered to 16Å.

Supervised classification (SC) (Valle et al. 2002) of nearly 60,000 particles using a wild type reference prepared from the X-ray structure of *E. coli* 30S (PDBID: 2AVY) and the reconstructed volume from particles picked from a subset of the micrographs (Step 1) showed an approximate 70:30 split between mature particles and another class containing roughly 17,000 particles (Step 1, Class 3), presumably representing incompletely assembled 30S subunits (Figure 12).

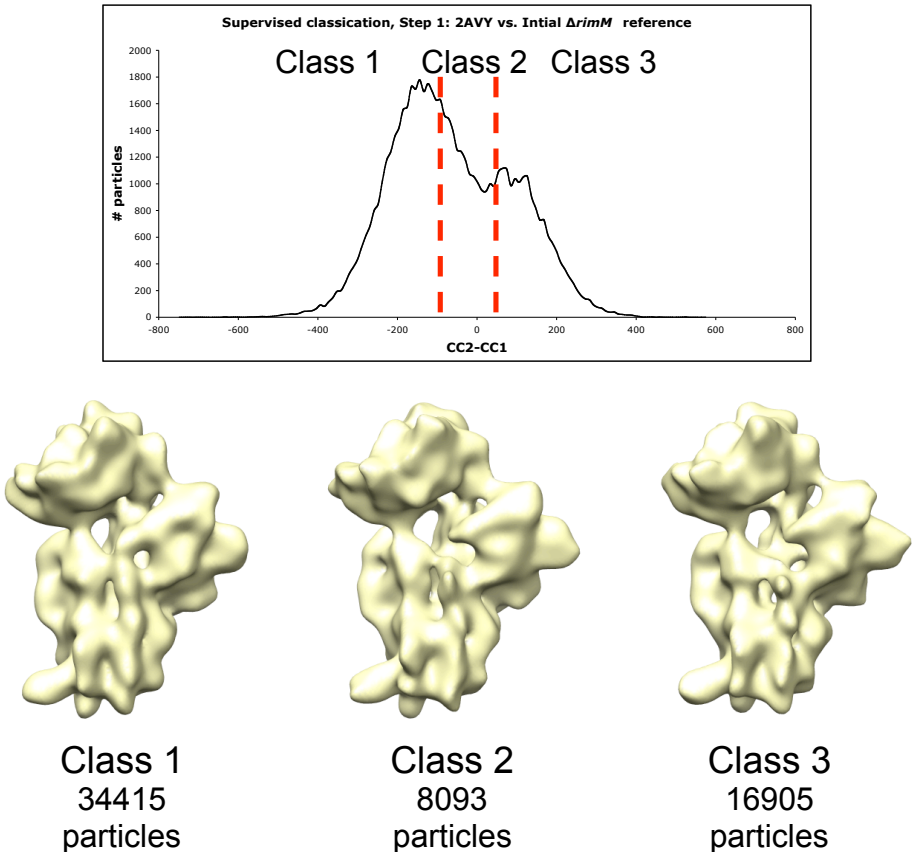

Figure 12: Supervised Classification of Δ*rimM* 30S. The histogram above shows the distribution of classification for the Δ*rimM* particles as a function of their cross-correlation (CC) coefficients against projections of Reference 1 (reference volume prepared from 2AVY) and Reference 2 (the initial reconstruction seen in Figure 11, representing Δ*rimM* 30S*)*. The Class 1 reconstruction includes the particles assigned higher cross-correlation with projections of the mature 30S, and the reconstructed volume resembles a mature 30S subunit. Particles more closely resembling the Δ*rimM* average volume have missing density at the decoding centre. The "mixed" particle population, Class 2, for which the difference in cross correlation scores was low, also appears to be more like the Δ*rimM*, or Class 3, model. This, and the poor peak resolution, suggests that the Supervised Classification is not completely efficient in differentiating immature particles from mature.

In an attempt to improve the immature map and discover any remaining heterogeneity, the particles from Step 1, Class 3 and additional particles from Class 2 (total 20,500) were used in Maximum Likelihood (ML) classification (Step 2), an unsupervised method of particle classification. Maximum Likelihood calculates the probably that each particle image resulted from a given seed volume, and weights their contribution to the calculated volume, accordingly. After multiple iterations, the probability of the calculated models having resulted in the experimental images is maximized (Scheres et al. 2007b). The resulting maps showed a structure atypical of mature 30S, suggesting that supervised classification had been mostly effective in sorting mature 30S particles from the dataset (Figure 13).

Assuming that the ML results could represent a better description of the immature subunit found in Δ*rimM*, the resulting map that appeared to have the least resemblance to the mature 30S was used as a reference in a second round of Supervised Classification of all particles (Step 3), which improved peak separation relative to Step 1 (Figure 14). The resulting map of the immature particle class had a calculated resolution of 18Å and showed features consistent with previous reconstructions, and is presented in Figure 14.

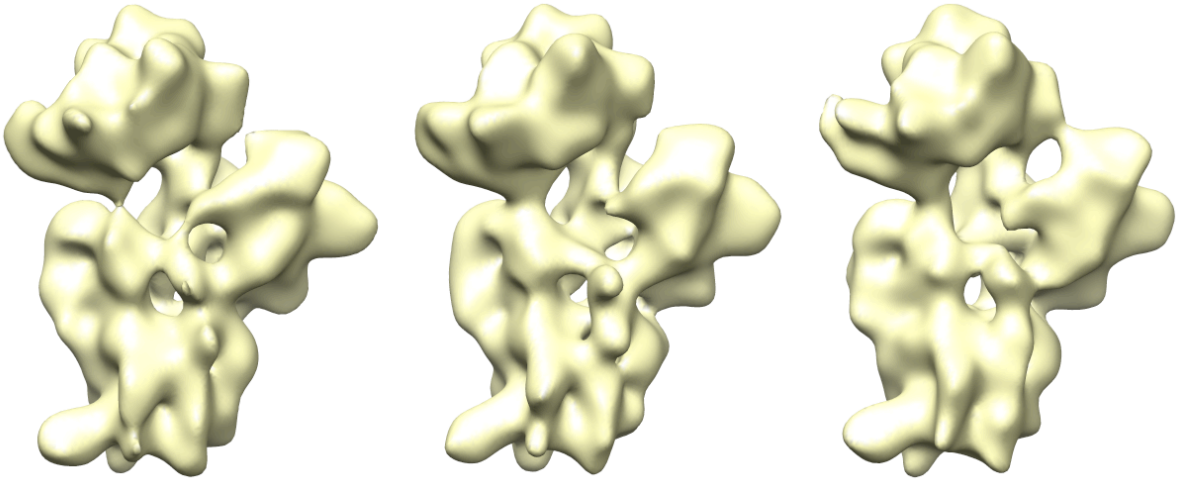

Figure 13: Results of Maximum Likelihood classification of the immature class resulting from the first Supervised Classification. The particles contributing to the map of the Δ*rimM* 30S subunit pictured in Figure 11, as well as some from Class 2 (for a total of 20,500 particles) were subjected to Maximum Likelihood classification in Xmipp. The three resulting maps have a resolution of approximately 22Å (FSC criterion 0.5). None of the maps exhibit a mature conformation at the decoding centre, suggesting that supervised classification effectively identified a majority of mature particles. The map at centre was used in a second round of supervised classification (Step 3, see Figure 14) to improve classification from the full particle dataset.

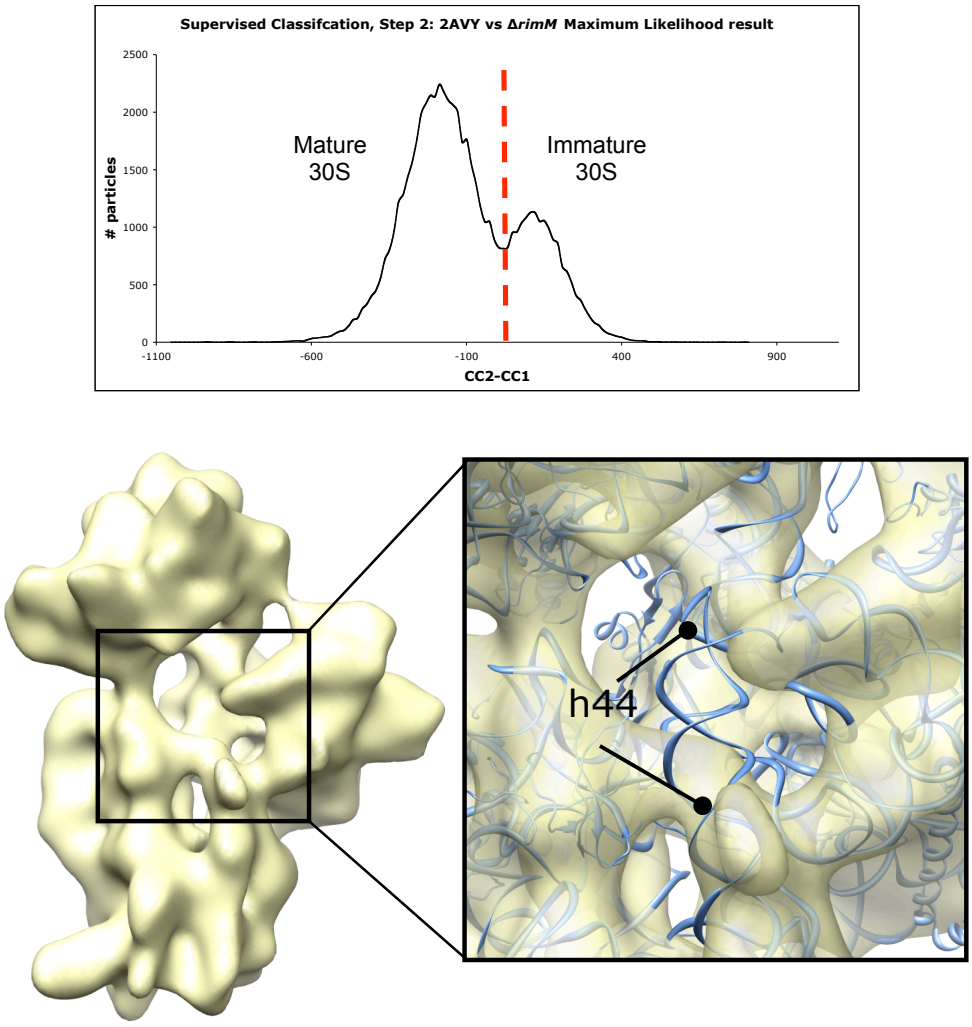

Figure 14: Model of the Δ*rimM* 30S subunit at 18Å. Reconstructed from immature particles identified in the second round of supervised classification using a Maximum Likelihood result as the immature reference (CC histogram above). A more definitive separation of two classes is shown by improved peak separation in cross-correlation difference. The 3D model of the immature 30S (15,720 particles) shows a profound distortion of helix 44, 45 and the decoding centre, similar to that of Δ*yjeQ* (Jomaa et al. 2011), where the 3' end of helix 44 extends perpendicular to the plane of the interface. The proper conformation of the decoding centre has no corresponding density in the EM map, as shown by the X-ray model fitting in the right panel. Such a conformation renders the decoding centre inactive, as well as interfering with binding to 50S. The X-ray structure of *E. coli* 30S (PDBID: 2AVY) was fit into the EM map using UCSF Chimera.

Difference mapping, shown in Figure 15, highlights dissimilar densities in the Δ*rimM* model versus the wild type EM model solved by Ahmad Jomaa (EMDB #1775) (Jomaa et al. 2011a). Most notably, the decoding centre of the Δ*rimM* 30S has missing densities at the decoding centre corresponding to the 3' end of the rRNA. The density that in wild type volumes corresponds to helix 45, or the 3' end of the small subunit rRNA, is absent from the model reconstructed from the particles from the Δ*rimM* strain.

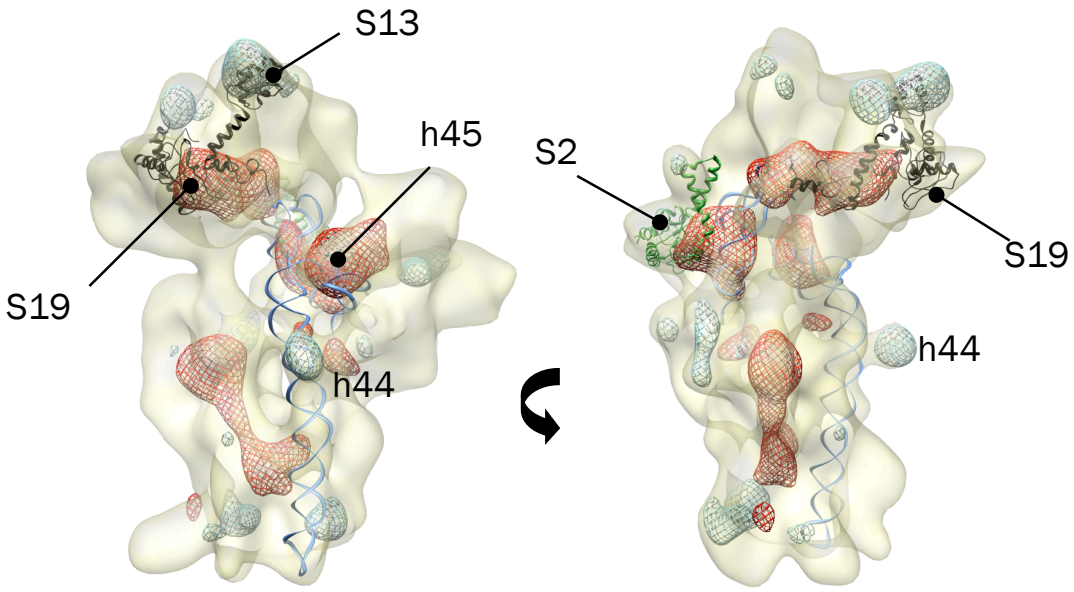

Figure 15: Difference maps of Δ*rimM* 30S versus wild type mature 30S (EMDB 1775). Difference maps prepared by subtracting one normalized EM volume highlight differing densities. Shown in red are densities occurring in the mature 30S, and in cyan are densities unique to the Δ*rimM* model. Helix 45 is not present in its mature conformation in the Δ*rimM* 30S as a consequence of displacement of the unprocessed 3' end of the rRNA, seen extending outward in the side view of the map (h44). Other densities through the head and neck suggest conformational differences in this region, either due to orientation and/or protein incorporation in the features labelled. Identification of most of the differing densities is uncertain at this resolution (18Å).

In the Δ*rimM* model, there is a density extending from helix 44 perpendicular to the plane of the interface, corresponding to the 3' end of the rRNA as it is displaced outward similar to Δ*yjeQ* (Figures 14 and 15) (Jomaa et al. 2011a). Such a conformation of the decoding centre and helices 44 and 45 disrupts not only translational activity, but also binding to the 50S subunits, accounting for the accumulation of 30S subunits in the *rimM* knockout. The difference map also shows changes in density through the neck and head region of the 30S, suggesting that these regions are not formed or oriented the same as in the mature subunit.

In the immature Δ*rimM* 30S, difference map density around protein S2 may indicate that the protein is underrepresented as it is in Δ*yjeQ* (Jomaa et al. 2011a) Recent, unpublished, bis/tris polyacrylamide gel analysis of r-protein complement of Δ*rimM* 30S by A. Jomaa and V. Leong suggests this is the case. Also of note are densities present in the Δ*rimM* 30S suggesting movement of S13 and S19 in the Δ*rimM* 30S subunit. These proteins bind close together on the interface side of the head, and S19 has been shown to interact with RimM (Lovgren et al. 2004).

4. DISCUSSION

Deletion of RimM from *E. coli* results in inefficient rRNA maturation and the accumulation of a 17S rRNA-containing 30S subunit. There is conflicting evidence as to whether 30S subunits containing immature rRNA can associate into 70S ribosomes, and as to the order and essentiality of the RNase processes in forming functional 30S subunits. In this work and in the previous study on the Δ*yjeQ* 30S, there is evidence that 30S subunits containing the 17S precursor to 16S rRNA are unable to associate into mature 70S ribosomes (Jomaa et al. 2011a), which causes free 30S subunits to accumulate as seen in the sucrose gradient profiles. The free 50S subunits result from a high demand for new ribosomes, but a lack of binding partners among the defective 30S subunits. Some of the difficulty in interpreting conflicting observations in other studies lies in identification of rRNA species using primer extension. That method maps the 5' end maturation state but not that of the 3' end, and complicates identification of 17S rRNA. Maturation of the 3' end seems to be required for both association into 70S ribosomes and formation of the decoding centre. Processing of the 3' end of 17S rRNA seems to occur before association with the 50S, while maturation of the 5' end may occur in polysomes (Hayes and Vasseur 1976; Jomaa et al. 2011a; Mangiarotti et al. 1974; Roy-Chaudhuri et al. 2010).

4.1 Free 30S subunits may be subject to degradation

Ribosome profiles at various optical densities show a loss of free 30S subunits in the BW25113 background, for both the Δ*rimM* knockout and the parental strain. Mature 16S rRNA levels appear to remain consistent according to gel analysis (Figure 9), while

17S rRNA levels decrease upon entry to the stationary phase, suggesting that the 16S rRNA incorporated into functional ribosomes is protected.

Previous studies have shown that when *E. coli* is starved for certain nutrients, the otherwise "stable" rRNA population is degraded (Davis et al. 1986; Deutscher 2003; Jacobson and Gillespie 1968; Okamura et al. 1973). At least one investigation showed that in cases of phosphate starvation, 30S subunits are degraded more readily than 50S (Davis et al. 1986). The ribosome profiles collected in exponential growth and in early stationary phase by Davis et al. show a similar trend to those in Figure 10. Other starvation studies limiting carbon and glucose did not observe a preferential degradation of 30S, but rather a decrease in all rRNA populations (30S, 50S, 70S, and polysomes) (Jacobson and Gillespie 1968; Okamura et al. 1973).

It must be noted that nearly complete starvation of nutrients and prolonged incubation times (>20 hours, up to 72 hours) are not equivalent conditions to the downshift of cells to stationary phase in gradually depleted LB medium. In cells allowed to grow to stationary phase in supplemented minimal medium, rRNA appears mostly stable until the transition to stationary phase. Cellular concentrations of both 23S and 16S rRNA are reduced before stabilizing at lower levels (Piir et al. 2011), which correlates with the similar relative levels of 16S and 23S seen throughout growth in the gel analysis in Figure 9. The study by Piir et al. did not investigate ribosome or polysome profiles.

Davis et al. hypothesize that 30S subunits in the free state—that is, without 50S partners or initiation factors (IFs) bound—are more susceptible to degradation (Davis et al. 1986). An accumulation of free subunits such as those in Δ*rimM* may therefore be

susceptible to, or even targeted for, degradation by cellular RNases as nutrients become limited. While the conditions for ribosome degradation in *E. coli* are not yet known in detail, degradation of nonfunctional ribosomes has been demonstrated in yeast (Cole et al. 2009; Fujii et al. 2009; LaRiviere et al. 2006). Quality control of unneeded or defective rRNA in bacteria may be accomplished by members of the same ribonuclease systems involved in mRNA degradation and rRNA maturation (Deutscher 2003; Deutscher 2006). Indeed, there is evidence that incorrectly processed rRNA containing precursor sequences can become polyadenylated, which could mark immature rRNA (such as 17S) and immature subunits for degradation (Li et al. 1998).

The evidence reviewed above presents a possible explanation for the disappearance of free 30S subunits in both the parental and the RimM knockout strains; cells degrade ribosomes and rRNA upon loss of nutrients and/or entry to stationary phase, and free 30S subunits may present a preferred target at the beginning of this process, particularly if they are not fully mature and functional. It is also possible that at least some of the free 30S are being incorporated into 70S ribosomes in both cases, despite the lack of obvious fluctuation of the 50S or 70S populations.

The ultimate fate of the accumulated 17S-containing 30S subunits during growth may be assessed by pulse-chase analysis of labelled rRNA (e.g. using tritiated uridine) in strain with inducible expression of RimM. Gel electrophoresis and analysis of signal intensity post-chase could reveal if the 17S rRNA population is incorporated into the 16S population or into degradation products such as the unknown 16S species seen in Δ*rimM* and Δ*yjeQ* ribosomal RNA samples (Figure 6). High rates of degradation in growing cells

would imply that the immature 30S accumulated in Δ*rimM* represents a dead-end product and not a *bona fide* assembly intermediate that can be rescued with induced RimM expression. In this case, the accumulated subunit may be the consequence of the true RimM substrate being modified by other factors, but then abandoned due to some other block to maturation that cannot be overcome by related factors such as RbfA, YjeQ and Era. Investigation of the structure of immature subunits found in viable double knockouts could be informative in this case.

It has been shown that over-expression of RbfA can partially recover the Δ*rimM* phenotype (Bylund et al. 1998). If in a pulse-chase experiment the Δ*rimM* 17S-containing subunits are degraded, their viability or lack thereof for maturation could also be assessed by induced over-expression of RbfA. RbfA may not, in fact, rescue the Δ*rimM* immature subunits, but rather could allow more efficient processing through a different pathway that is not otherwise favoured during normal growth with a full repertoire of assembly factors. Thus, it may be of interest to investigate not only complementation of Δ*rimM* with induced expression of RimM, both in pulse-chase rRNA analysis and ribosome profiles, but also introduction of an induced excess of RbfA to assess the fate of immature subunits in Δ*rimM*.

4.2 The Δ*rimM* 30S subunit has a defective decoding centre

The immature 30S subunit accumulated in Δ*rimM E. coli* appears to have a displaced decoding centre as a consequence of inefficient rRNA maturation (Figures 14 and 15). Like Δ*yjeQ*, the missing density at the top of helix 44 corresponds with a density extending perpendicular to the plane of the interface, presumably the unprocessed 3' end

of the 17S rRNA. Without the ability to monitor the match between the mRNA codon and tRNA anticodon, and without the B2a contact point needed to associate with 50S subunits (Mitchell et al. 1992; Schuwirth et al. 2005), this conformation is non-functional. This finding offers additional evidence that 3' maturation is a key step in the assembly of functional 30S subunits.

An earlier study on a Δ*rimM* strain reported that the 70S ribosomes in those cells had reduced translational efficiency (Bylund et al. 1997), while a more recent publication also linked RimM deletion to increased read-through of stop codons (Roy-Chaudhuri et al. 2010), suggesting that deletion of RimM and subsequent defects in assembly affected the functionality of "mature" ribosomes. It is possible that not all of the variance in the neck and head is attributable to the presence of the immature rRNA, and that differences persist in the Δ*rimM* 30S even if the 16S is produced and the 30S is competent to bind 50S and to decode mRNA. The neck of the 30S is flexible in mature subunits and in the binary 70S complex, and may play a role in decoding fidelity (Zaher and Green 2009). Assembly of the neck is influenced by assembly of the body and the head (Calidas and Culver 2011). Differences in these regions could affect otherwise functional ribosomes. Protein-content analysis and cryo-EM of Δ*rimM* 30S subunits from 70S ribosomes could reveal any differences from those in the parental strain.

The small number of particles and low resolution (18Å) of the Δ*rimM* immature map makes it difficult to interpret the model or the difference maps with sufficient accuracy. Consequently, the identification of small densities in the difference map remains mostly speculative. The true localization of differing features and their fit with

corresponding X-ray structures must be improved by increasing the size of the dataset. In the future, a larger dataset should also be further analyzed *in silico* to assess further heterogeneity that cannot be resolved with a small dataset of fewer than 16,000 immature particles. Corroborating mass spectrometry data on the relative levels of r-proteins in the Δ*rimM* versus the wild type would also be valuable in assessing the model, as it was with Δ*yjeQ* (Jomaa et al. 2011a). Some small differences at the positions of S19 and S13 and the interior of the head correspond with the supposed role of RimM in facilitating proper assembly of the 3' major domain. In reconstitution experiments with single assembly factors, binding of RimM to the 30S also appears to retard binding of S13, perhaps by physically blocking its corporation (Bunner et al. 2010b). RimM could facilitate proper conformation of the S13 binding area prior to release of RimM from the assembling 30S subunit.

The similarity of the Δ*rimM* 30S to structures at the decoding centre of the Δ*yjeQ* 30S, in the general area where YjeQ and RbfA are known to bind (Datta et al. 2007;Jomaa et al. 2011b) and where RimM may also localize (Lovgren et al. 2004) lends support to a semi-concerted model for late 30S subunit assembly, in which these and related factors such as Era associate with a similar immature state of the 30S and interact with it and each other to achieve final maturation of the decoding centre. The Δ*rimM* reconstruction and that of Δ*yjeQ* do not appear to be completely identical, and may have slightly differing r-protein complements and conformation. Nevertheless, it is apparent from both of these models that YjeQ and RimM act in late assembly, and that delayed

processing of the 3' end of the 16S rRNA has functional and structural consequences for the 30S subunit.

Era interacts with h45 (Sharma et al. 2005; Tu et al. 2011), which is displaced in the Δ*rimM* 30S and probably in the Δ*yjeQ* 30S (Jomaa et al. 2011a), which may indicate that it associates after h45 is in place or guides it to that position, or that related assembly factors bound together induce a different conformation that has not yet been observed. The recent structures of the Δ*ksgA* 30S and the KsgA:30S co-structure indicated that the methylation of helix 45 may occur after the other factors act to facilitate 3' maturation and guide h45 to its mature location in the platform (Boehringer et al. 2012). It may be important to note that these assembly factor:30S co-structures contain mature 16S rRNA, and that the interactions described in these studies could represent only the post-3'-maturation interactions of these factors with the 30S subunit.

A recent cryo-EM study of small subunit assembly in *Saccharomyces cerevisiae* showed an array of assembly factors bound to the pre-40S, including the KsgA homolog Dim1 and the 3' endonuclease for which the bacterial homolog is unknown (Strunk et al. 2011). This demonstrates that, at least in yeast, multiple assembly factors occupy the assembling subunit. In the multi-factor:pre-40S complex, helix 44 is displaced and the decoding centre is disrupted in a similar fashion to the Δ*rimM* 30S, the Δ*yjeQ* 30S, and the co-structure with RbfA (Datta et al. 2007; Jomaa et al. 2011a). In both the eukaryotic and bacterial models, one of the functions of the assembly factors may be to prevent association with the large subunit. The distortion of h44 seen when assembly factors are

bound may contribute to this regulation, and/or render the 3' end accessible for maturation.

Whether the interaction of late-acting assembly factors follows a sequential or concerted model or both, a map of binding interdependency, like that for the r-proteins, may be developed for a more accurate view of the native binding conformation and contribution of each assembly factor *in vivo*, and the maturation state of the ribosome upon which they act.

4.3 Difficulty resolving sample heterogeneity

In the ideal case, an electron microscopy reconstruction of a biological molecule is derived from a homogeneous sample, such that the particle images represent differing views of identical objects. Both purification limitations and intrinsic flexibility of some biological macromolecules present a challenge in obtaining such ideal samples that will not introduce uncertainty into averaged models. A variety of tools in image processing have been developed both to overcome heterogeneity and to take advantage of the information offered in identifying conformational differences (Leschziner and Nogales 2007). Deleting assembly factors such as YjeQ and RimM demonstrably enriches the numbers of incompletely processed 30S subunits in the cell (Jomaa et al. 2011a) (Figures 6 and 7). However free 30S from a viable, growing bacterial strain necessarily include mature or nearly-mature subunits, no matter how enriched the immature subunits. Biochemical means of separating distinct populations of subunits that have the same sedimentation coefficient have thus far not been developed in our lab. *In silico* methods

of differentiating different states of similar molecules have been developed (Scheres et al. 2007a; Valle et al. 2002), and were employed in this study.

Supervised classification of the 30S subunits collected from Δ*rimM* showed that in comparing a wild type reference derived from the X-ray structure (PDB ID: 2AVY) and an average model of the Δ*rimM* particles, the classification was not entirely able to differentiate some particle images. In addition to poor peak separation, reconstructions using particles with only slightly differing coefficients (e.g. ΔCC ±40) resulted in a 3D model that more resembled an immature structure than one with an intact decoding centre (Figure 12), suggesting that some immature particles may be misclassified as ambiguous or even mature. Misclassification could be a consequence of unsuitable models, perhaps because the Δ*rimM* model was not representative, or because it was simply too similar to wild type to generate disparate cross correlations. Alternatively, searching for only two states of the 30S subunit left a third conformation to ambiguous classification.

Supervised classification using the wild type 30S EM volume (EMDB 1775) as a reference versus the Δ*rimM* reference generates a unimodal distribution of ΔCC scores (Figure 16). Splitting the dataset into four classes along the distribution results in a mature-looking 30S structure and three other classes with varying degrees of distortion of helix 44. The fourth model, Class 1, derived from the "most wild type" particles in which the density forming helix 44 does not appear to meet that of r-protein S12 (Figure 16). This may indicate a certain flexibility of h44 in the Δ*rimM* 30S subunit, or that there is another conformation of the 30S in the sample that is not resolved in classification using these references. Indeed, such a case may be responsible for the apparent disagreement

between the rRNA analysis (~50% of ΔrimM 16S rRNA is unprocessed), and the classification findings (the majority of the particles appear more mature).

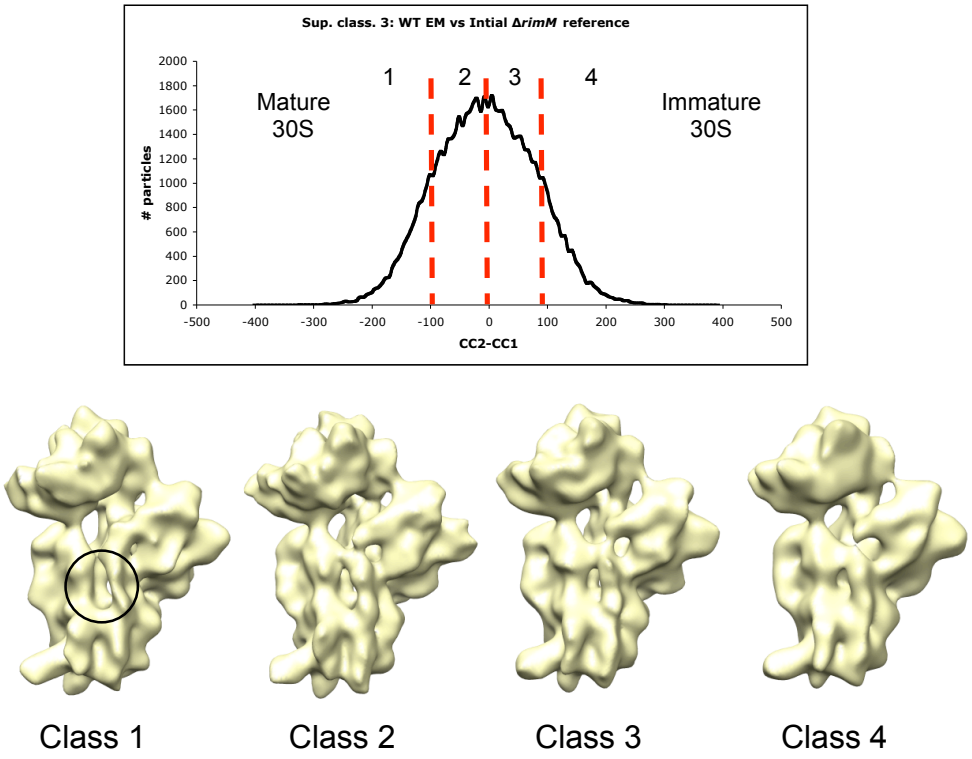

Figure 16: Reconstructions resulting from Supervised Classification using a wild type EM structure as a reference. The unimodal curve (above) resulting from a Supervised Classification using EMDB 1775 and the Δ*rimM* initial reference results in poor classification of particles and resolution of different populations. Models derived from particles that are most immature-like (Classes 3 and 4) show narrow density at the decoding centre, indicative of mixed conformations. The leftmost structure arising from those particles scored most like mature 30S seem to lack density in the region of S12 where it typically merges with the density of h44 (circled).

Maximum Likelihood classification, as outlined in Results, is an unsupervised method for which the number of solutions is limited by the number of seed volumes chosen by the user, rather than by resemblance to one of two references. Using ML on all ~60,000 particle images results in one volume from 16,189 particles that resembled the

mature 30S, and three other volumes that appeared to be immature to some extent, with narrowing volumes at the decoding centre as well as slight differences possibly associated with the 5' end of the rRNA (Figure 17). These results may also indicate difficulty in differentiating a subtle difference in the mature 30S versus that of Δ*rimM*.

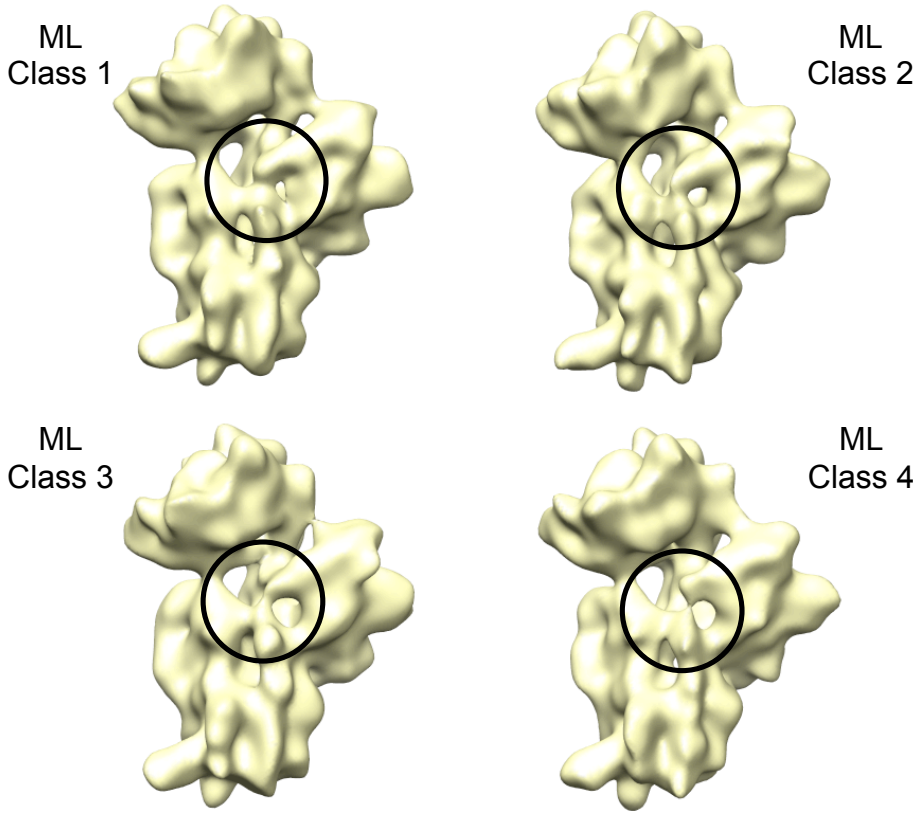

Figure 17: Maximum Likelihood classification results from 59,413 Δ*rimM* particles. The reconstruction labelled Class 1 most closely resembles a mature 30S subunit, with all landmark structures including the upper portion of helix 44 (the decoding centre) in position and intact as indicated by the circle. Class 2 shows only slight conformational differences and a narrowing of the h44 density. This narrowing becomes more pronounced in Classes 3 and 4. Flexibility in this region may be one of the factors complicating classification of homogeneous populations in the sample. All maps in this figure are low-pass filtered to a resolution of 19Å.

A common finding throughout classification efforts using both Supervised Classification and Maximum Likelihood was the persistence of structures with narrow

densities at the decoding centre, where the initial Δ*rimM* reconstruction had none (note that such structures also largely lack density corresponding to h45). This may indicate remaining heterogeneity in the sample; that is, particles for which h44 is in its functional position are introducing density to the structure that cannot fully resolved due to averaging. It was observed after fitting the X-ray crystal structure into these models that the density could correspond with the 5' strand of h44 as it descends from the neck. At model resolutions ranging from 17 to 22 Ångstroms is it difficult to determine this with any certainty. Maximum Likelihood classification is the method preferred to resolve small conformational changes, but given the results seen here, ML may work better with a larger dataset, or, if h44 is truly flexible, with particles with more defined conformational states. Nevertheless, distortion of h44 appears to be a hallmark of the 30S subunits accumulated in Δ*rimM*, given that variable density or lack thereof was observed in results from Supervised Classification using a variety of references, and in reference-free Maximum Likelihood classification.

In summary, this thesis presents results confirming that the inefficient maturation of 17S rRNA leads to accumulation of immature 30S subunits, and that these subunits have a non-functional conformation due to a disrupted decoding centre and the misposition of helix 44 and h45. This additional evidence that an immature conformation of helix 44 is a feature of late assembly contributes to the emerging model of 30S assembly, in which maturation of the 3' end of the rRNA is a crucial step before translational competence and which may be facilitated by multiple late-acting factors.

5. REFERENCES

Aebi U, Pollard TD. 1987. A glow discharge unit to render electron microscope grids and other surfaces hydrophilic. *J. Electron Microsc. Tech.* **7**: 29-33.

Anantharaman V, Aravind L. 2002. The PRC-barrel: a widespread, conserved domain shared by photosynthetic reaction center subunits and proteins of RNA metabolism. *Genome Biol.* **3**: RESEARCH0061.

Baba T, Ara T, Hasegawa M, Takai Y, Okumura Y, Baba M, Datsenko KA, Tomita M, Wanner BL, Mori H. 2006. Construction of *Escherichia coli* K-12 in-frame, single-gene knockout mutants: the Keio collection. *Mol. Syst. Biol.* **2**: 2006.0008.

Ban N, Nissen P, Hansen J, Moore PB, Steitz TA. 2000. The complete atomic structure of the large ribosomal subunit at 2.4 Å resolution. *Science* **289**: 905-920.

Boehringer D, O'Farrell HC, Rife JP, Ban N. 2012. Structural insights into methyltransferase KsgA function in 30S ribosomal subunit biogenesis. *J. Biol. Chem.*

Bunner AE, Beck AH, Williamson JR. 2010a. Kinetic cooperativity in *Escherichia coli* 30S ribosomal subunit reconstitution reveals additional complexity in the assembly landscape. *Proc. Natl. Acad. Sci. U. S. A.*

Bunner AE, Nord S, Wikstrom PM, Williamson JR. 2010b. The effect of ribosome assembly cofactors on in vitro 30S subunit reconstitution. *J. Mol. Biol.* **398**: 1-7.

Bylund GO, Persson BC, Lundberg LA, Wikstrom PM. 1997. A novel ribosome-associated protein is important for efficient translation in *Escherichia coli*. *J. Bacteriol.* **179**: 4567-4574.

Bylund GO, Wipemo LC, Lundberg LA, Wikstrom PM. 1998. RimM and RbfA are essential for efficient processing of 16S rRNA in *Escherichia coli*. *J. Bacteriol.* **180**: 73-82.

Calidas D, Culver GM. 2011. Interdependencies govern multidomain architecture in ribosomal small subunit assembly. *RNA* **17**: 263-277.

Campbell TL, Brown ED. 2008. Genetic interaction screens with ordered overexpression and deletion clone sets implicate the *Escherichia coli* GTPase YjeQ in late ribosome biogenesis. *J. Bacteriol.* **190**: 2537-2545.

Champney WS. 1977. Kinetics of ribosome synthesis during a nutritional shift-up in *Escherichia coli* K-12. *Mol. Gen. Genet.* **152**: 259-266.

Cole SE, LaRiviere FJ, Merrikh CN, Moore MJ. 2009. A convergence of rRNA and mRNA quality control pathways revealed by mechanistic analysis of nonfunctional rRNA decay. *Mol. Cell* **34**: 440-450.

Connolly K, Culver G. 2009. Deconstructing ribosome construction. *Trends Biochem. Sci.* **34**: 256-263.

Connolly K, Rife JP, Culver G. 2008. Mechanistic insight into the ribosome biogenesis functions of the ancient protein KsgA. *Mol. Microbiol.* **70**: 1062-1075.

Daigle DM, Brown ED. 2004. Studies of the interaction of *Escherichia coli* YjeQ with the ribosome in vitro. *J. Bacteriol.* **186**: 1381-1387.

Daigle DM, Rossi L, Berghuis AM, Aravind L, Koonin EV, Brown ED. 2002. YjeQ, an essential, conserved, uncharacterized protein from *Escherichia coli*, is an unusual GTPase with circularly permuted G-motifs and marked burst kinetics. *Biochemistry* **41**: 11109-11117.

Dammel CS, Noller HF. 1995. Suppression of a cold-sensitive mutation in 16S rRNA by overexpression of a novel ribosome-binding factor, RbfA. *Genes Dev.* **9**: 626-637.

Datta PP, Wilson DN, Kawazoe M, Swami NK, Kaminishi T, Sharma MR, Booth TM, Takemoto C, Fucini P, Yokoyama S et al. 2007. Structural aspects of RbfA action during small ribosomal subunit assembly. *Mol. Cell* **28**: 434-445.

Davis BD, Luger SM, Tai PC. 1986. Role of ribosome degradation in the death of starved Escherichia coli cells. *J. Bacteriol.* **166**: 439-445.

de Narvaez CC, Schaup HW. 1979. In vivo transcriptionally coupled assembly of *Escherichia coli* ribosomal subunits. *J. Mol. Biol.* **134**: 1-22.

Deutscher MP. 2003. Degradation of stable RNA in bacteria. *J. Biol. Chem.* **278**: 45041-45044.

Deutscher MP. 2006. Degradation of RNA in bacteria: comparison of mRNA and stable RNA. *Nucleic Acids Res.* **34**: 659-666.

Fujii K, Kitabatake M, Sakata T, Miyata A, Ohno M. 2009. A role for ubiquitin in the clearance of nonfunctional rRNAs. *Genes Dev.* **23**: 963-974.

Goto S, Kato S, Kimura T, Muto A, Himeno H. 2011. RsgA releases RbfA from 30S ribosome during a late stage of ribosome biosynthesis. *EMBO J.* **30**: 104-114.

Grishin NV. 2001. KH domain: one motif, two folds. *Nucleic Acids Res.* **29**: 638-643.

Grondek JF, Culver GM. 2004. Assembly of the 30S ribosomal subunit: positioning ribosomal protein S13 in the S7 assembly branch. *RNA* **10**: 1861-1866.

Guo Q, Yuan Y, Xu Y, Feng B, Liu L, Chen K, Sun M, Yang Z, Lei J, Gao N. 2011. Structural basis for the function of a small GTPase RsgA on the 30S ribosomal subunit maturation revealed by cryoelectron microscopy. *Proc. Natl. Acad. Sci. U. S. A.* **108**: 13100-13105.

Hase Y, Yokoyama S, Kimura T, Goto S, Muto A, Himeno H. 2009. Physiological role of RsgA in ribosome biosynthesis. *Nucleic Acids Symp. Ser. (Oxf)* **(53)**: 307-308.

Hayes F, Vasseur M. 1976. Processing of the 17-S *Escherichia coli* precursor RNA in the 27-S pre-ribosomal particle. *Eur. J. Biochem.* **61**: 433-442.

Held WA, Ballou B, Mizushima S, Nomura M. 1974. Assembly mapping of 30 S ribosomal proteins from Escherichia coli. Further studies. *J. Biol. Chem.* **249**: 3103-3111.

Helser TL, Davies JE, Dahlberg JE. 1972. Mechanism of kasugamycin resistance in *Escherichia coli*. *Nat. New Biol.* **235**: 6-9.

Himeno H, Hanawa-Suetsugu K, Kimura T, Takagi K, Sugiyama W, Shirata S, Mikami T, Odagiri F, Osanai Y, Watanabe D et al. 2004. A novel GTPase activated by the small subunit of ribosome. *Nucleic Acids Res.* **32**: 5303-5309.

Holmes KL, Culver GM. 2004. Mapping structural differences between 30S ribosomal subunit assembly intermediates. *Nat. Struct. Mol. Biol.* **11**: 179-186.

Inoue K, Alsina J, Chen J, Inouye M. 2003. Suppression of defective ribosome assembly in a *rbfA* deletion mutant by overexpression of Era, an essential GTPase in *Escherichia coli*. *Mol. Microbiol.* **48**: 1005-1016.

Inoue K, Chen J, Tan Q, Inouye M. 2006. Era and RbfA have overlapping function in ribosome biogenesis in *Escherichia coli*. *J. Mol. Microbiol. Biotechnol.* **11**: 41-52.

Jacobson A, Gillespie D. 1968. Metabolic events occurring during recovery from prolonged glucose starvation in *Escherichia coli*. *J. Bacteriol.* **95**: 1030-1039.

Jomaa A, Stewart G, Martin-Benito J, Zielke R, Campbell TL, Maddock JR, Brown ED, Ortega J. 2011a. Understanding ribosome assembly: the structure of in vivo assembled immature 30S subunits revealed by cryo-electron microscopy. *RNA*.

Jomaa A, Stewart G, Mears JA, Kireeva I, Brown ED, Ortega J. 2011b. Cryo-electron microscopy structure of the 30S subunit in complex with the YjeQ biogenesis factor. *RNA* **17**: 2026-2038.

LaRiviere FJ, Cole SE, Ferullo DJ, Moore MJ. 2006. A late-acting quality control process for mature eukaryotic rRNAs. *Mol. Cell* **24**: 619-626.

Leschziner AE, Nogales E. 2007. Visualizing flexibility at molecular resolution: analysis of heterogeneity in single-particle electron microscopy reconstructions. *Annu. Rev. Biophys. Biomol. Struct.* **36**: 43-62.

Li Z, Pandit S, Deutscher MP. 1998. Polyadenylation of stable RNA precursors in vivo. *Proc. Natl. Acad. Sci. U. S. A.* **95**: 12158-12162.

Li Z, Pandit S, Deutscher MP. 1999. RNase G (CafA protein) and RNase E are both required for the 5' maturation of 16S ribosomal RNA. *EMBO J.* **18**: 2878-2885.

Lindahl L. 1975. Intermediates and time kinetics of the *in vivo* assembly of *Escherichia coli* ribosomes. *J. Mol. Biol.* **92**: 15-37.

Lovgren JM, Bylund GO, Srivastava MK, Lundberg LA, Persson OP, Wingsle G, Wikstrom PM. 2004. The PRC-barrel domain of the ribosome maturation protein RimM mediates binding to ribosomal protein S19 in the 30S ribosomal subunits. *RNA* **10**: 1798-1812.

Lu Q, Inouye M. 1998. The gene for 16S rRNA methyltransferase (ksgA) functions as a multicopy suppressor for a cold-sensitive mutant of Era, an essential RAS-like GTP-binding protein in *Escherichia coli*. *J. Bacteriol.* **180**: 5243-5246.

Ludtke SJ, Baldwin PR, Chiu W. 1999. EMAN: semiautomated software for high-resolution single-particle reconstructions. *J. Struct. Biol.* **128**: 82-97.

Maguire BA. 2009. Inhibition of bacterial ribosome assembly: a suitable drug target? *Microbiol. Mol. Biol. Rev.* **73**: 22-35.

Mangiarotti G, Turco E, Ponzetto A, Altruda F. 1974. Precursor 16S RNA in active 30S ribosomes. *Nature* **247**: 147-148.

Mindell JA, Grigorieff N. 2003. Accurate determination of local defocus and specimen tilt in electron microscopy. *J. Struct. Biol.* **142**: 334-347.

Mitchell P, Osswald M, Brimacombe R. 1992. Identification of intermolecular RNA cross-links at the subunit interface of the *Escherichia coli* ribosome. *Biochemistry* **31**: 3004-3011.

Mizushima S, Nomura M. 1970. Assembly mapping of 30S ribosomal proteins from *E. coli*. *Nature* **226**: 1214.

Mulder AM, Yoshioka C, Beck AH, Bunner AE, Milligan RA, Potter CS, Carragher B, Williamson JR. 2010. Visualizing ribosome biogenesis: parallel assembly pathways for the 30S subunit. *Science* **330**: 673-677.

O'Farrell HC, Pulicherla N, Desai PM, Rife JP. 2006. Recognition of a complex substrate by the KsgA/Dim1 family of enzymes has been conserved throughout evolution. *RNA* **12**: 725-733.

Okamura S, Maruyama HB, Yanagita T. 1973. Ribosome degradation and degradation products in starved *Escherichia coli*. VI. Prolonged culture during glucose starvation. *J. Biochem.* **73**: 915-922.

Piir K, Paier A, Liiv A, Tenson T, Maivali U. 2011. Ribosome degradation in growing bacteria. *EMBO Rep.* **12**: 458-462.

Poldermans B, Roza L, Van Knippenberg PH. 1979. Studies on the function of two adjacent N6, N6-dimethyladenosines near the 3' end of 16S ribosomal RNA of *Escherichia coli*. III. Purification and properties of the methylating enzyme and methylase-30S interactions. *J. Biol. Chem.* **254**: 9094-9100.

Roy-Chaudhuri B, Kirthi N, Culver GM. 2010. Appropriate maturation and folding of 16S rRNA during 30S subunit biogenesis are critical for translational fidelity. *Proc. Natl. Acad. Sci. U. S. A.* **107**: 4567-4572.

Scheres SH, Gao H, Valle M, Herman GT, Eggermont PP, Frank J, Carazo JM. 2007a. Disentangling conformational states of macromolecules in 3D-EM through likelihood optimization. *Nat. Methods* **4**: 27-29.

Scheres SH, Gao H, Valle M, Herman GT, Eggermont PP, Frank J, Carazo JM. 2007b. Disentangling conformational states of macromolecules in 3D-EM through likelihood optimization. *Nat. Methods* **4**: 27-29.

Scheres SH, Nunez-Ramirez R, Sorzano CO, Carazo JM, Marabini R. 2008. Image processing for electron microscopy single-particle analysis using XMIPP. *Nat. Protoc.* **3**: 977-990.

Schuwirth BS, Borovinskaya MA, Hau CW, Zhang W, Vila-Sanjurjo A, Holton JM, Cate JH. 2005. Structures of the bacterial ribosome at 3.5 Å resolution. *Science* **310**: 827-834.

Shajani Z, Sykes MT, Williamson JR. 2011. Assembly of bacterial ribosomes. *Annu. Rev. Biochem.* **80**: 501-526.

Sharma MR, Barat C, Wilson DN, Booth TM, Kawazoe M, Hori-Takemoto C, Shirouzu M, Yokoyama S, Fucini P, Agrawal RK. 2005. Interaction of Era with the 30S ribosomal subunit implications for 30S subunit assembly. *Mol. Cell* **18**: 319-329.

Srivastava AK, Schlessinger D. 1990. Mechanism and regulation of bacterial ribosomal RNA processing. *Annu. Rev. Microbiol.* **44**: 105-129.

Strunk BS, Loucks CR, Su M, Vashisth H, Cheng S, Schilling J, Brooks CL,3rd, Karbstein K, Skiniotis G. 2011. Ribosome assembly factors prevent premature translation initiation by 40S assembly intermediates. *Science* **333**: 1449-1453.

Suzuki S, Tatsuguchi A, Matsumoto E, Kawazoe M, Kaminishi T, Shirouzu M, Muto Y, Takemoto C, Yokoyama S. 2007. Structural characterization of the ribosome maturation protein, RimM. *J. Bacteriol.* **189**: 6397-6406.

Talkington MW, Siuzdak G, Williamson JR. 2005. An assembly landscape for the 30S ribosomal subunit. *Nature* **438**: 628-632.

Traub P, Nomura M. 1968. Structure and function of E. coli ribosomes. V. Reconstitution of functionally active 30S ribosomal particles from RNA and proteins. *Proc. Natl. Acad. Sci. U. S. A.* **59**: 777-784.

Tu C, Zhou X, Tarasov SG, Tropea JE, Austin BP, Waugh DS, Court DL, Ji X. 2011. The Era GTPase recognizes the GAUCACCUCC sequence and binds helix 45 near the 3' end of 16S rRNA. *Proc. Natl. Acad. Sci. U. S. A.* **108**: 10156-10161.

Valle M, Sengupta J, Swami NK, Grassucci RA, Burkhardt N, Nierhaus KH, Agrawal RK, Frank J. 2002. Cryo-EM reveals an active role for aminoacyl-tRNA in the accommodation process. *EMBO J.* **21**: 3557-3567.

Wilson DN, Nierhaus KH. 2007. The weird and wonderful world of bacterial ribosome regulation. *Crit. Rev. Biochem. Mol. Biol.* **42**: 187-219.

Wimberly BT, Brodersen DE, Clemons WM,Jr, Morgan-Warren RJ, Carter AP, Vonrhein C, Hartsch T, Ramakrishnan V. 2000. Structure of the 30S ribosomal subunit. *Nature* **407**: 327-339.

Wireman JW, Sypherd PS. 1974. *In vitro* assembly of 30S ribosomal particles from precursor 16S RNA of *Escherichia coli*. *Nature* **247**: 552-554.

Xia B, Ke H, Shinde U, Inouye M. 2003. The role of RbfA in 16S rRNA processing and cell growth at low temperature in *Escherichia coli*. *J. Mol. Biol.* **332**: 575-584.

Zaher HS, Green R. 2009. Fidelity at the molecular level: lessons from protein synthesis. *Cell* **136**: 746-762.